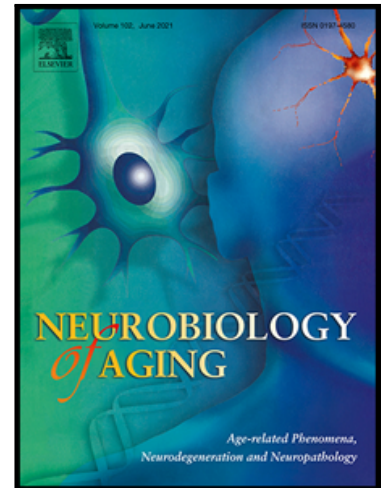


## Journal Pre-proof

Association of plasma  $A\beta_{40}/A\beta_{42}$  ratio and brain  $A\beta$  accumulation: testing a whole-brain PLS-VIP in individuals at risk of Alzheimer's disease

Pablo Lemercier MSc , Andrea Vergallo MD , Simone Lista PhD , Henrik Zetterberg MD, PhD , Kaj Blennow MD , Marie-Claude Potier PhD , Marie-Odile Habert MD , François-Xavier Lejeune PhD , Bruno Dubois MD , Stefan Teipel MD , Harald Hampel MD, PhD , for the INSIGHT-preAD study group the Alzheimer Precision Medicine Initiative (APMI)



PII: S0197-4580(21)00229-3  
DOI: <https://doi.org/10.1016/j.neurobiolaging.2021.07.005>  
Reference: NBA 11200

To appear in: *Neurobiology of Aging*

Received date: 17 March 2021  
Revised date: 25 June 2021  
Accepted date: 7 July 2021

Please cite this article as: Pablo Lemercier MSc , Andrea Vergallo MD , Simone Lista PhD , Henrik Zetterberg MD, PhD , Kaj Blennow MD , Marie-Claude Potier PhD , Marie-Odile Habert MD , François-Xavier Lejeune PhD , Bruno Dubois MD , Stefan Teipel MD , Harald Hampel MD, PhD , for the INSIGHT-preAD study group the Alzheimer Precision Medicine Initiative (APMI), Association of plasma  $A\beta_{40}/A\beta_{42}$  ratio and brain  $A\beta$  accumulation: testing a whole-brain PLS-VIP in individuals at risk of Alzheimer's disease, *Neurobiology of Aging* (2021), doi: <https://doi.org/10.1016/j.neurobiolaging.2021.07.005>

This is a PDF file of an article that has undergone enhancements after acceptance, such as the addition of a cover page and metadata, and formatting for readability, but it is not yet the definitive version of record. This version will undergo additional copyediting, typesetting and review before it is published in its final form, but we are providing this version to give early visibility of the article. Please note that, during the production process, errors may be discovered which could affect the content, and all legal disclaimers that apply to the journal pertain.

© 2021 Published by Elsevier Inc.

## Association of plasma A $\beta$ 40/A $\beta$ 42 ratio and brain A $\beta$ accumulation: testing a whole-brain PLS-VIP in individuals at risk of Alzheimer's disease

Pablo Lemercier<sup>a,#,\*</sup> [pablo.lemercier@inserm.fr](mailto:pablo.lemercier@inserm.fr), MSc, Andrea Vergallo<sup>a,#</sup>, MD, Simone Lista<sup>a</sup>, PhD, Henrik Zetterberg<sup>b,c,d,e</sup>, MD, PhD, Kaj Blennow<sup>b,c</sup>, MD, Marie-Claude Potier<sup>f</sup>, PhD, Marie-Odile Habert<sup>g,h,i</sup>, MD, François-Xavier Lejeune<sup>j</sup>, PhD, Bruno Dubois<sup>a</sup>, MD, Stefan Teipel<sup>k</sup>, MD, and Harald Hampel<sup>a</sup> [harald.hampel@med.uni-muenchen.de](mailto:harald.hampel@med.uni-muenchen.de), MD, PhD, for the INSIGHT-preAD study group, and the Alzheimer Precision Medicine Initiative (APMI)

<sup>a</sup>Sorbonne University, GRC n° 21, Alzheimer Precision Medicine (APM), AP-HP, Pitié-Salpêtrière Hospital, Boulevard de l'hôpital, F-75013, Paris, France

<sup>b</sup>Department of Psychiatry and Neurochemistry, Institute of Neuroscience & Physiology, the Sahlgrenska Academy at the University of Gothenburg, Mölndal, Sweden

<sup>c</sup>Clinical Neurochemistry Laboratory, Sahlgrenska University Hospital, Mölndal, Sweden

<sup>d</sup>Department of Neurodegenerative Disease, UCL Institute of Neurology, Queen Square, London, UK.

<sup>e</sup>UK Dementia Research Institute at UCL, London, UK.

<sup>f</sup>ICM Institut du Cerveau et de la Moelle épinière, CNRS UMR7225, INSERM U1127, UPMC, Hôpital de la Pitié-Salpêtrière, 47 Bd de l'Hôpital, F-75013 Paris, France.

<sup>g</sup>Sorbonne Université, CNRS, INSERM, Laboratoire d'Imagerie Biomédicale, F-75013, Paris, France.

<sup>h</sup>Centre pour l'Acquisition et le Traitement des Images ([www.cati-neuroimaging.com](http://www.cati-neuroimaging.com)), Paris, France.

<sup>i</sup>AP-HP, Hôpital Pitié-Salpêtrière, Département de Médecine Nucléaire, F-75013, Paris, France.

<sup>j</sup>Bioinformatics and Biostatistics Core Facility iCONICS, Inserm U 1127, CNRS UMR 7225, Sorbonne Université UMR S 1127, Institut du Cerveau et de La Moelle Épinière, Paris, France.

<sup>k</sup>Clinical Dementia Research Section, German Center for Neurodegenerative Diseases (DZNE), Rostock, Germany; Department of Psychosomatic Medicine, University Medicine Rostock, Rostock, Germany.

(+) equal contribution to the study.

**\*Correspondence to:**

*Pablo Lemercier, MSc & Harald Hampel, MD, PhD, MA, MSc*

*Sorbonne University Clinical Research Group (GRC n°21)*

*"Alzheimer Precision Medicine (APM)"*

*Établissements Publics à caractère Scientifique et Technologique (E.P.S.T.)*

Alzheimer Precision Medicine Initiative (APMI)  
<https://www.apmiscience.com/>

Phone: +33 1 57 27 46 74

Fax: +33 1 57 27 46 74

E-Mail: (P. Lemercier)

E-Mail: (H. Hampel)

### **HIGHLIGHTS**

- We investigated subjective memory complaints, a condition at increased risk of AD
- We used an innovative statistical approach enabling a whole-brain exploration
- Plasma A $\beta$ 42/40 ratio associates with A $\beta$  accumulation in networks generally not investigated in preclinical AD
- Our approach is free from a-priori hypothesis constraints
- Our whole-brain approach allows to investigate early pathophysiological changes of AD

### **Abstract**

Molecular and brain regional/network-wise pathophysiological changes at preclinical stages of Alzheimer's disease (AD) have primarily been found through knowledge-based studies conducted in late-stage mild cognitive impairment/dementia populations. However, such an approach may compromise the objective of identifying the earliest spatial-temporal pathophysiological processes.

We investigated 261 individuals with subjective memory complaints, a condition at increased risk of AD, to test a whole-brain, non-a-priori method based on partial least squares, in unraveling the association between plasma A $\beta$ 42/A $\beta$ 40 ratio and an extensive set of brain regions characterized through molecular imaging of A $\beta$  accumulation and cortical metabolism. Significant associations were mapped onto large-scale networks, identified through an atlas and by knowledge, to elaborate on the reliability of the results.

Plasma A $\beta$ 42/40 ratio was associated with A $\beta$ -PET uptake (but not FDG-PET) in regions generally investigated in preclinical AD such as those belonging to the default mode network, but also in regions/networks normally not accounted - including the central

executive and salience networks - which likely have a selective vulnerability to incipient A $\beta$  accumulation.

The present whole-brain approach is promising to investigate early pathophysiological changes of AD to fully capture the complexity of the disease, which is essential to develop timely screening, detection, diagnostic, and therapeutic interventions.

## Keywords

Subjective memory complaints, Preclinical Alzheimer's disease, Plasma amyloid  $\beta$ , Partial least square, whole-brain

Abbreviations: Alzheimer's disease (AD)

## INTRODUCTION

Brain accumulation of amyloid- $\beta$  (A $\beta$ ) aggregation species is one of the earliest pathophysiological alterations in the preclinical phase of the Alzheimer's disease (AD) clinical-biological continuum (Bateman et al., 2012; Jack et al., 2018; Villemagne et al., 2013). From a therapeutic perspective, the early detection of incipient A $\beta$  accumulation and downstream co-occurring alterations, such as spreading of tau pathology, synaptic failure, and neurodegeneration, holds the potential to effectively intervene using targeted disease-modifying therapies that can slow down AD disease progression during preclinical or prodromal stages (Aisen et al., 2017; Hampel et al., 2019a). ~~On the flip side~~ By contrast, individuals at risk for AD or any other neurodegenerative disease may have different clinical-biological trajectories with some developing brain resilience, at the molecular and network level, ~~and some other going toward~~ while other individuals may develop multi-scale system failure and cognitive decline (Arenaza-Urquijo and Vemuri, 2018; Elman et al., 2014; Perez-Nievas et al., 2013). Therefore, reliable multi-modal exploratory and integrative approaches are needed for investigating network dysfunction in AD trajectories but also resilience in individuals displaying incipient molecular signatures of AD or any other neurodegenerative disease.

Positron emission tomography (PET) studies have shown that the regional A $\beta$  accumulation in preclinical AD or individuals at genetic/clinical risk for AD is associated with different predictors, including bodily fluid biomarkers (McKhann et al., 2011). Coupling these findings with functional magnetic resonance imaging (MRI) studies and experimental models of AD revealed that a selective vulnerability of distinct brain regions to AD incipient

pathophysiology exists. However, A $\beta$  PET-based studies in preclinical AD typically employ a-priori, knowledge-based selected regions of interest (ROIs) such as the hippocampus, the anterior and posterior cingulate, or the precuneus (Fan et al., 2018; Fandos et al., 2017; Nakamura et al., 2018; Pérez-Grijalba et al., 2019; Vergallo et al., 2019). A limitation of this approach is represented by the fact that most of these regions have been identified in studies conducted in populations with more advanced stages of AD-like mild cognitive impairment (MCI) and dementia. Using approaches that constrain the number of hypotheses tested may hinder the comprehensive understanding of early AD pathophysiological dynamics. A model capable of accounting for a broad set of aging and AD-vulnerable regions is urgently needed to tackle incipient pathophysiological alterations timely.

Novel approaches that allow investigating more brain regions and different hubs of large-scale networks without a-priori constraints are needed in preclinical AD studies to develop timely screening, diagnostic, and therapeutic strategies. An ideal knowledge-free method should limit type 1 error inflation - induced by an increased number of hypotheses to test - and should deal with multicollinearity. This is of significant relevance since neuroimaging studies revealed significant pairwise correlations of AD hallmarks, like amyloid- $\beta$  and also tau proteinopathies, between different regional values (Lockhart et al., 2017; Veronese et al., 2019).

In the present study, we investigated a non-a-priori design (i.e., hypothesis-free) based on Partial Least Square (PLS) analysis, a statistical method that allows an exploratory whole-brain approach. PLS estimates principal components, maximizing the covariance within and between two tables of the same set of observations to find shared information (Abdi and Williams, 2013). PLS is a component-based tool with several advantages compared to univariate methods, including higher suitability for modeling of datasets with considerable collinearity among variables. We employed the Variable Importance in Projection (VIP) criteria applied to PLS (PLS-VIP) to select the most relevant hypothesis. Indeed, simulation studies showed that PLS-VIP outperforms other variable selection methods and is less sensitive to noise and collinearity (Chong and Jun, 2005; Palermo et al., 2009).

We tested the PLS-VIP approach by investigating the association of plasma A $\beta$ <sub>42</sub>/A $\beta$ <sub>40</sub> ratio, a validated biomarker for screening of AD pathophysiology (Jack et al., 2018; Nakamura et al., 2018; Palmqvist et al., 2019; Vergallo et al., 2019), with whole-brain A $\beta$ -PET regional indexes. We used multi-modal biomarkers charting the A $\beta$  pathway about which several studies have corroborated a significant covariance between different modality

measures (i.e., blood concentrations and molecular imaging indexes). Such a confidence in the relationship between the two set of variables is pivotal for the scope of the present article, which consists in testing the reliability of a PLS-based methodological approach.

Previous studies in preclinical and prodromal AD showed good to optimal accuracy of plasma A $\beta$ 42/A $\beta$ 40 ratio in predicting A $\beta$ -PET status (positive versus negative) (Nakamura et al., 2018; Palmqvist et al., 2019). Moreover, a correlation between the former and global/regional A $\beta$ -PET standard uptake value ratios (SUVRs) has been reported across different AD cohorts (Fandos et al., 2017; Nakamura et al., 2018; Vergallo et al., 2019).

To test the conceptual validity of our model, we also tested plasma A $\beta$ 42/A $\beta$ 40 ratio association with <sup>18</sup>F-fluorodeoxyglucose (FDG) regional radiotracer binding, a marker of neuronal metabolism, assuming no relation would stand out as the existing literature suggests. We investigated this non-a-priori approach in a cohort of cognitively intact individuals facing subjective memory complaints (SMC), a clinical condition characterized by normal performance at a multi-domain neuropsychometric assessment despite a self-perceived memory impairment (Buckley et al., 2016; Teipel et al., 2020; Timmers et al., 2019; van Harten et al., 2018). Several multi-centric and multi-modal biomarkers studies indicate that SMC, coupled with positivity to A $\beta$  biomarkers, is associated with increased risk of developing MCI or dementia within the clinical spectrum of AD (Buckley et al., 2016; Teipel et al., 2020; Timmers et al., 2019; van Harten et al., 2013). While this association is consistent across studies, partially controversial is the link between SMC and common risk factors for dementia – including vascular pathology and or tau pathophysiology (Clancy et al., 2021; Dubois et al., 2018; Van Etten et al., 2020).

We carried out our research proposal in the INSIGHT-preAD study cohort, a well-defined, large-scale, observational, monocentric, university-based longitudinal cohort of individuals with SMC and no significant medical comorbidities (see below for more details).

## **MATERIALS AND METHODS**

### **Study participants**

The study sample consisted of 318 participants with subjective memory complain (SMC), who were enrolled in the standardized, large-scale, observational, monocentric, French academic university-based “INveStIGATION of AlzHeimer’s PredicTors in Subjective Memory Complainers” (INSIGHT-preAD) study (Dubois et al., 2018) – that is part of the Alzheimer Precision Medicine Initiative (APMI) and its established Cohort Program (APMI-

CP) (Hempel et al., 2019b) . Participants were enrolled at the Institute of Memory and Alzheimer's disease (Institut de la Mémoire et de la Maladie d'Alzheimer, IM2A) at the Pitié-Salpêtrière University Hospital in Paris, France. The main objective of the INSIGHT-preAD study is to explore the earliest preclinical stages of AD through intermediate to later stages until progression to conversion to first cognitive symptoms, using comprehensive clinical parameters and biomarkers associated with cognitive decline. In brief, the INSIGHT-preAD study includes 318 cognitively and physically healthy white (Caucasian) individuals, recruited from the community in the wider Paris area, France, aged 70 to 85, with SMC.

SMC was defined as a positive response (“YES”) to both of the following questions: “Are you complaining about your memory?” and “Is it a regular complaint that has lasted for more than 6 months?” All participants were required to have an intact cognitive function – defined as a Mini-Mental State Examination score (MMSE)  $\geq 27$ , a Clinical Dementia Rating scale (CDR) of 0, and a Free and Cued Selective Rating Test (FCSRT) total recall score  $\geq 41$ .

A $\beta$ -PET investigation was performed at the baseline visit, as a mandatory inclusion criterion. Thus, all subjects enrolled into the study have SMC and are stratified as either positive or negative for cerebral A $\beta$  deposition. At the point of the study inclusion, several data were collected, namely demographic and clinical data, and Apolipoprotein E (APOE) genotype (see Supplementary materials for more details).

Exclusion criteria were a history of neurological or psychiatric diseases, including depressive disorders. Medical conditions, potential causing cognitive decline of non-AD biological nature, were ruled out at baseline (see Dubois et al., 2018 for more details). The study was conducted following the tenets of the Declaration of Helsinki of 1975 and approved by the local Institutional Review Board at the participating center. All participants or their representatives gave written informed consent to use their clinical data for research purposes.

### **Blood sample and plasma immunoassay**

Ten (10) mL of venous blood was collected in 1 BD Vacutainer® lithium heparin tube, which was used for all subsequent immunochemical analyses. Blood samples were taken in the morning, after a 12-hour fast, handled in a standardized way, and centrifuged for 15 minutes at 2000 G-force at 4°C. Per sample, plasma fraction was collected, homogenized, aliquoted into multiple 0.5 mL cryovial-sterilized tubes, and finally stored at -80°C within 2 hours from collection.

Analyses of plasma A $\beta$ <sub>42</sub> and A $\beta$ <sub>40</sub> concentrations were performed at the Clinical Neurochemistry Laboratory, Sahlgrenska University Hospital, Sweden. In particular, a volume of 0.5 mL of plasma for each subject was required for performing the analyses using the platforms mentioned above. Plasma A $\beta$ <sub>1-42</sub> and A $\beta$ <sub>1-40</sub> were analyzed using the Single-molecule array (Simoa) immunoassay (Quanterix, Billerica, Lexington, MA, USA). Regarding A $\beta$ <sub>42</sub>, repeatability was 4.1% and intermediate precision 7.0% for an internal QC plasma sample with a concentration of 10.5 pg/mL. Regarding A $\beta$ <sub>40</sub>, repeatability was 4.0% and intermediate precision 6.4% for an internal QC plasma sample with a concentration of 203 pg/mL.

### **PET scan acquisition and processing**

A $\beta$  and <sup>18</sup>F-FDG-PET investigations were performed at the baseline visit (M0) – as part of the inclusion criteria – and at two-year follow-up (M24). Both scans were acquired in separate sessions, with a 48 hours interval.

Brain A $\beta$ -PET scans were acquired 50 minutes after injection of 370 MBq (10 mCi) of <sup>18</sup>F-Florbetapir, which has high affinity for amyloid plaques. Brain <sup>18</sup>F-FDG scans were obtained 30 minutes after injection of 2 MBq/kg of 2-deoxy-2-(<sup>18</sup>F)fluoro-D-glucose (<sup>18</sup>F-FDG). All acquisitions were performed in a single session on a Philips Gemini GXL scanner and consisted of 3 × 5 minutes frames with a voxel size of 2 × 2 × 2 mm<sup>3</sup>. Images were then reconstructed using an iterative LOR-RAMLA algorithm (10 iterations), with a “smooth” post-reconstruction filter. All corrections (attenuation, scatter and random coincidence) were integrated into the reconstruction. Lastly, frames were realigned, averaged, and quality-checked by the CATI team (*Centre d'Acquisition et Traitement des Images*; <http://cati-neuroimaging.com>). CATI is a French neuroimaging platform (available at <http://cati-neuroimaging.com>). PET images were then analyzed with an in-house pipeline developed by the CATI, including partial volume effect correction, as previously described (Dubois et al., 2018; Habert et al., 2018).

Finally, standard uptake value ratios (SUVR) were calculated using as reference regions a composite volume of interest (ROI) including pons and the whole cerebellum for Florbetapir images, whereas the pons for FDG images. SUVR were obtained in 84 cortical and neocortical ROIs extrapolated through Automated Anatomical Labeling (AAL) atlas. The global A $\beta$ -PET SUVR was calculated as the average of the 84 cortical ROIs similarly as previously described in Farrell et al., 2018; Landau et al., 2010; Whittington et al., 2018.

## Statistical analysis

### *Preprocessing strategy*

A robust approach for variable selection, widely used in data science (Hastie et al., 2009; Xu and Goodacre, 2018), consists of dividing the dataset into a training set, used for selecting the variables, and a testing set, used to evaluate the selection. This latter provides an unbiased assessment of the variable selection procedure and, thus, enhances the confidence in the findings. To this end, we randomly split the dataset into a training and a testing dataset with a ratio of 1:1 stratifying by age, sex, *APOE*  $\epsilon$ 4 allele, education level, and total intracranial volume (TIV).

We reported descriptive statistics for the strata variables in the split datasets using the mean and standard deviation (SD) for quantitative variables and the frequency counts and percentages for categorical variables. We used Student's t-tests or chi-squared tests to evaluate the sampling homogeneity at a significance level of  $p < 0.05$ .

In the sequel, the training dataset was used for the PLS-VIP selection of the most relevant association between the regional PET signal and the plasma  $A\beta_{42}/A\beta_{40}$  ratio, thus reducing the number of hypotheses. Then, the test data set was used to further validate the remaining assumptions.

### *Correlation between ROIs*

First, we conducted correlation analyses on the training dataset to explore how imaging measurements were related across the different brain sub-regions according to the two PET techniques. To this end, for each pair of the 84  $A\beta$ -PET (as well as FDG-PET) ROIs, we calculate the Pearson's correlations of the SUVR. Histograms and boxplots were build up to represent distributions of the pairwise correlation coefficients obtained with  $A\beta$ -PET and FDG-PET data.

### *Data modeling and feature selection*

Associations between plasma  $A\beta_{42}/A\beta_{40}$  ratio and either regional  $A\beta$ -PET SUVR or FDG-PET were determined through PLS models (Wold et al., 1993), on the training dataset (one model was fitted for each PET technique). Based on the NIPALS (Non-Linear iterative Partial Least Square) algorithm, PLS is a dimension reduction method, which is well-suited for managing high levels of correlations like, in the present study, between regional PET

measures. In PLS, the X-matrix of imaging data can be reduced to a subset of orthogonal latent variables (or components), where each latent variable is constructed as a weighted sum of the X-variables, maximizing the covariance with the variable Y of A $\beta$ 42/A $\beta$ 40 ratios.

For feature selection, the method combining PLS and the variable importance in projection (VIP) scores (also called PLS-VIP method) have been introduced to detect the most influential predictors in explaining the variation of the Y-variable (Chong and Jun, 2005). Based on the PLS components, a VIP score can be calculated for each sub-region to quantify its contribution to the variance explained by the component (Mehmood et al., 2012; Wold et al., 1993). Predictors with large VIP, larger than 1, are commonly the most relevant for explaining Y (Chong and Jun, 2005).

To achieve a stable selection, we used a bootstrap procedure to compute the VIP scores. Average VIP scores were thus calculated for each sub-region based on 5000 models obtained from bootstrap versions of the original dataset. Finally, the averaged VIP scores, sorted by descending values, were used to select and rank the most associated regions. For each PET technique, the PLS-VIP method was performed using the R package mixOmics (Chong and Jun, 2005; Rohart et al., 2017) specifying the “canonical mode” with one PLS component for the PLS model. To avoid confounding effects of age, sex, *APOE*  $\epsilon$ 4 carriers, and education level the training dataset were pre-processed prior to modeling with the ComBat method (Johnson et al., 2007) implemented in the R package sva available at <https://bioconductor.org/packages>.

McNemar chi-squared test was used to check for lateralized dominance between hemispheres for the selected regions.

### **Validation**

The selected regions were further assessed for association with the plasma biomarkers using data of the testing set with no pre-processing. This was done through linear regression models (one model for each selected sub-region used as the dependent variable) to test the predicting effect of plasma A $\beta$ 42/A $\beta$ 40 ratio adjusted for the covariates age, sex, and *APOE*  $\epsilon$ 4 genotype.

For each model, the A $\beta$ 42/A $\beta$ 40 ratio coefficient was reported with standard error (SE), and p-value. The Cohen’s  $f^2$  value was also calculated to indicate the effect size of A $\beta$ 42/A $\beta$ 40. Finally, all p-values obtained for A $\beta$ 42/A $\beta$ 40 were corrected using False

Discovery Rate (FDR) for multiple testing, and its association with a sub-region was confirmed when the adjusted p-value was smaller than 0.05.

### ***Internal reproducibility***

As no independent cohort was available, we assessed the reproducibility of our method on data collected at months 12 (M12) and M24. We expected to find the same regions as previously identified. Besides, ~~this allowed us to investigate the~~ since some associations may vanish over time, it inquires sustainability of the identified associations during the subjects' follow-up period.

Thus, we replicated the same procedure described above for selecting and validating the regions at the longitudinal level with data at M12 and M24 with the same split samples used at M0. We tested A $\beta$  accumulation and metabolism over a 1-year follow-up using plasma A $\beta$ 42/A $\beta$ 40 ratio measure at M12 and PET SUVRs at M24. Similarly, we tested A $\beta$  accumulation and neuronal metabolism over a 2-year follow-up using plasma A $\beta$ 42/A $\beta$ 40 ratio measured at baseline and PET measured at M24.

### ***Confounding analysis***

As regional A $\beta$ -PET SUVR and plasma A $\beta$ 42/A $\beta$ 40 can be influenced by the total amount of A $\beta$  accumulation in patients, we conducted a confounding analysis to test whether the association between regional A $\beta$ -PET SUVR and plasma A $\beta$ 42/A $\beta$ 40 can be explained by the brain overall amount of A $\beta$  accumulation. This question was addressed at a cross-sectional level by using structural equation modeling (SEM) on the testing dataset. SEM is a convenient approach to model at the same time the relationships between regional A $\beta$  and plasma A $\beta$ 42/A $\beta$ 40, between global A $\beta$  and plasma A $\beta$ 42/A $\beta$ 40 and between regional and global A $\beta$ .

All models (one model by sub-region), including the covariates age, sex and *APOE*  $\epsilon$ 4 genotype, were built with the R package lavaan (Rosseel, 2012). We calculated p-values on all plasma A $\beta$ 42/A $\beta$ 40, global and regional A $\beta$ -PET SUVR based on models fitted with 5000 bootstrap replicates of the original testing set. Finally, we corrected the p-values for controlling the FDR, and all associations remaining without the confounding effect of the total A $\beta$  accumulation were established for all regions with an adjusted p-value < 0.05.

### ***Interpretation of the PLS results-relevance through knowledge-based functional networks***

We performed a matching between the ROIs selected by the PLS and a knowledge-driven selection of large-scale networks, typically impaired in AD, to assist in the interpretation of the PLS-based results and gain more insights on whether the approach we employed may represent viable methodological solution for future clinical research studies in the field of aging and AD.

The definition of functional network components was made by grouping regions based on resting-state network atlas (Shirer et al., 2012), available at [https://findlab.stanford.edu/functional\\_ROIs.html](https://findlab.stanford.edu/functional_ROIs.html)). We selected networks that have hypothesized functions in AD-related pathology: auditory network (AN), default mode network (DMN), central executive network (CEN), salience network (SaN), sensorimotor network (SeN), and visual network (VN). We matched the cortical regions of the AAL atlas and the resting-state network atlas based on our knowledge and visual inspection (see Supplementary Table S1 for more details).

Cohen's kappa ( $\kappa$ ) with 95% confidence interval (95% CI) was used to assess agreement between selected ROIs and each brain large-scale functional network. Cohen's kappa is commonly used for quantifying agreement between two sets of binary classification tasks, considering that the agreement may occur by chance (Warrens, 2015).

All statistical analyses were performed with R software, version 3.6.0 (R Development Core Team, 2019) and plots were generated with the ggplot2 package (Wickham, 2009). Feature selection using PLS-VIP and confounding analyses were performed respectively with the R packages mixOmics (Rohart et al., 2017), available at <https://bioconductor.org/packages>, and lavaan (Rosseel, 2012), available at <http://cran.r-project.org/web/packages>. A script is supplied to allow the reader to apply our method (see Supplementary material).

## RESULTS

### Datasets description

Analyses were performed on the 261 participants from the INSIGHT-preAD cohort who completed structural MRI, A $\beta$ -PET, and FDG-PET acquisition at study inclusion.

Demographic characteristics, *APOE*  $\epsilon$ 4 genotype subgroups, and TIV are summarized for the training and the test datasets in **Table 1**. We did not find any significant difference between the two datasets regarding sex, *APOE*  $\epsilon$ 4 allele, age, education level, or TIV (p-values > 0.39). The distributions of the stratifying variables in the training and test sets are

provided in the supplementary material (**Figure S1**). Because of the good accordance of data, we considered both datasets were homogeneous for the subject sampling.

## Regional A $\beta$ accumulation

### *Cross-sectional study*

A $\beta$ -PET SUVR showed significant pairwise correlations with cortical regions (**Figure 1A**). Indeed, the regional pairwise correlation ranged from 0.58 to 0.99 with a median of 0.87.

Out of the 84 cortical structures investigated with bootstrapped PLS-VIP, the averaged VIP scores highlighted a subset of 34 regions with a score above 1 (**Table 2**). Most of these regions were located in the frontal cortex, the cingulate cortex, the bilateral precuneus, and the right insula. We observed that the selected regions are mainly located in the left hemisphere (see Supplementary material for more details). From the testing dataset, we observed a significant negative association between A $\beta$ 42/A $\beta$ 40 ratio and all the regions previously selected (**Table 2**). These associations remained valid after corrections for multiple testing. The values of Cohen's  $f^2$  ranging from 0.04 to 0.15 indicated a small to medium effect size of plasma A $\beta$ 42/A $\beta$ 40.

Interestingly, the confounding analysis highlighted the significant association of seven regions with the plasma A $\beta$ 42/A $\beta$ 40 ratio, which has been characterized after controlling for the confounding effect of the global A $\beta$ -PET SUVR. These regions concerned the bilateral medial cingulate, the left posterior cingulate, the right inferior frontal orbital, the right frontal superior medial, the left superior parietal, and the left precuneus (**Table S1**).

### *Longitudinal study*

The 1-year follow-up was assessed using A $\beta$ 42/A $\beta$ 40 ratio at M12 and A $\beta$ -PET imaging at M24. Bootstrapped PLS-VIP analysis selected 25 of the 84 regions (**Table 3**). These regions were mainly located in the frontal cortex and the cingulate cortex, including the bilateral insula. Likewise, the 2-year follow-up investigation on A $\beta$ 42/A $\beta$ 40 ratio at M0 and A $\beta$ -PET imaging at M24 selected 19 of the 84 regions (**Table 4**) mainly located in the frontal cortex and the cingulate cortex including right insula. Results showed a left hemisphere dominance for the 1-year follow-up analysis but not the 2-year follow-up (see Supplementary material for more details).

On the testing dataset, we observed a significant negative association between A $\beta$ 42/A $\beta$ 40 ratio and amyloid-PET in all the regions selected over a 1-year follow-up (**Table**

3) and a 2-year follow-up (**Table 4**). Besides, all of these results survived after FDR correction. Cohen's  $f^2$  values revealed a small to medium effect size of plasma A $\beta$ 42/A $\beta$ 40 over a 1-year follow-up and a small effect size of plasma A $\beta$ 42/A $\beta$ 40 over a 2-year follow-up.

## Regional cortical metabolism

### *Cross-sectional study*

Measures of cortical FDG-PET showed significant pairwise correlations with cortical regions (**Figure 1B**). The minimum regional pairwise correlation was 0.50, the maximum was 0.98, and the median 0.82.

Bootstrapped PLS-VIP selected 16 regions over 84 (**Table 5**). These regions were mainly located in the temporal cortex. Investigation on the testing dataset showed that A $\beta$ 42/A $\beta$ 40 ratio was not significantly associated with FDG-PET measure in any of these regions (**Table 5**).

### *Longitudinal study*

Bootstrapped PLS-VIP investigation on FDG-PET imaging at M24 identified 21 regions associated with baseline A $\beta$ 42/A $\beta$ 40 ratio and 16 regions with M12 A $\beta$ 42/A $\beta$ 40 ratio. Investigation on the testing dataset showed that A $\beta$ 42/A $\beta$ 40 ratio was not significantly associated with regional FDG-PET measure over a 1-year (**Table S2-S3**) or a 2-year follow-up (**Table S3-S4**).

## Selected regions and functional networks

Here we investigated whether selected A $\beta$ -PET regions at different follow-up visits were involved in specific resting state networks (see Supplementary Table S1 for more details). At baseline, the A $\beta$ -PET regional subset predominantly overlapped the CEN ( $\kappa = 0.46$ ; 95% CI = [0.27 - 0.65]) and the DMN ( $\kappa = 0.30$ ; 95% CI = [0.09 - 0.51]) (**Figure 2A**). The amyloid-PET regional subset selected at one-year follow-up, predominantly overlapped the CEN ( $\kappa = 0.37$ ; 95% CI = [0.16 - 0.59]) and the SaN ( $\kappa = 0.26$ ; 95% CI = [0.05 - 0.46]) (**Figure 2B**). Likewise, the two-year follow-up amyloid-PET regional subset predominantly overlapped the CEN ( $\kappa = 0.27$ ; 95% CI = [0.04 - 0.49]) and the SaN ( $\kappa = 0.27$ ; 95% CI = [0.03 - 0.5]) (**Figure 2C**).

## DISCUSSION

This study probes the potential clinical value of a whole-brain, non-a-priori approach based on PLS-VIP by investigating the association between plasma levels of A $\beta$ 42/A $\beta$ 40 ratio and an extensive set of regions characterized for A $\beta$  accumulation and cortical metabolism.

We used multi-modal biomarkers charting the A $\beta$  pathway, which is a valuable tool to explore our approach since several studies have corroborated a significant covariance between different modality measures (i.e., blood concentrations and molecular imaging indexes).

### *The PLS-VIP feature selection*

PLS-VIP method allows comprehensive exploration of brain single ROIs and hubs of large-scale networks that are likely to be involved in preclinical/early prodromal stages of AD. Most of the conventional study designs using knowledge-based a priori selection of ROIs may fail to capture several particularly vulnerable regions biologically connected to incipient AD pathophysiological events, including early stages of proteinopathies.

To probe our approach, we used data generated in a population of cognitively healthy individuals with SMC, a clinical condition associated with increased risk of AD (Buckley et al., 2016; van Harten et al., 2018). At baseline, we found that plasma A $\beta$ 42/A $\beta$ 40 ratio was negatively associated with A $\beta$ -PET indexes in the frontal cortex, the cingulate cortex, the precuneus, and the insula. The solutions delivered by PLS-VIP were consistent when the analysis was reproduced on the same cohort at different timepoints, indicating a robust and stable approach.

In the present study we confirmed the previously reported association between fluid biological signatures of the A $\beta$  pathway and A $\beta$ -PET signal in regions typically picked by a-priori study designs, such as the hippocampus, the anterior and posterior cingulate, or the precuneus (Fandos et al., 2017; Nakamura et al., 2018; Pérez-Grijalba et al., 2019). Moreover, we also identify additional regions vulnerable to AD pathophysiology, including the insula, the angular gyrus, and frontal cortex, as pointed out by previous ROI-based studies (Fan et al., 2018; Vergallo et al., 2019).

### *A preliminary selected ROI – knowledge-based network matching*

Finally, we conducted a stepwise knowledge-driven process to check whether the identified A $\beta$ -PET ROIs, including those who remained after controlling for global SUVR, matched with specific brain large-scale networks. We observed that the majority of regions whose A $\beta$  accumulation rates correlate with plasma A $\beta$ 42/A $\beta$ 40 ratio belonged to distinct macroscale networks either typically investigated in AD (DMN) or usually not taken into account for association studies (salience network (SaN), central executive network (CEN)), although their decline over age has been extensively reported (Agosta et al., 2012; Badhwar et al., 2017; Chiesa et al., 2020; Hampel et al., 2019a; Zhao et al., 2019).

There is consolidated evidence about the ~~impairment~~ of the DMN functional connectivity decline ~~in the DMN~~ and its association with AD pathophysiological hallmarks during the disease's early stages (Badhwar et al., 2017; Bero et al., 2011; Palmqvist et al., 2017; Teipel et al., 2016).

Functional MRI in-human studies indicate that there is spatial-temporal overlap between DMN activity decay and deposition A $\beta$  and tau (Hampel et al., 2019a; Li et al., 2019; Mormino et al., 2011) and that a decreased functional connectivity in the DMN is associated with neurodegeneration (Chhatwal et al., 2018; Palmqvist et al., 2017), cortical shrinking (Hampton et al., 2020) and worse cognitive trajectories in individuals displaying elevated A $\beta$  burden (Buckley et al., 2017).

~~This evidence in humans is supported by experimental models of aging and AD that point out the intrinsic bio-energetic vulnerability of the DMN neurons (Bero et al., 2011).~~

~~Evidence about an increased A $\beta$ -PET signal within the less studied CEN and the SaN (Grothe and Teipel, 2016; Myers et al., 2014; Palmqvist et al., 2017), throughout the biological continuum of AD and in aging stems from multi-modal imaging studies. Spatial covariance between A $\beta$  accumulation and connectivity and metabolism in the CEN (decreased) has been reported in aging and AD individuals (Andrews-Hanna et al., 2007; Grothe and Teipel, 2016; Palmqvist et al., 2017). A decreased functional connectivity has been reported within the SaN in aged individuals and patients suffering from early AD in which networks breakdown take place at different temporal coordinates (Brier et al., 2012; He et al., 2014; Zhou et al., 2010). Moreover, in this putative trickle-down effect, some dysfunctional networks may have a tight functional interconnection as indicated by studies reporting that the SaN serves to identify salient stimuli and modulates the functional switch between the DMN and the CEN (Crossley et al., 2014). Thus, disruption of the SaN characterized by impaired modulation of DMN and CEN activity was reported in MCI~~

compared to healthy elderly individuals (Chen et al., 2016). Furthermore, disruption in SaN modulation strength on DMN and CEN correlates with worse cognitive performance (Chand et al., 2017; He et al., 2014). Therefore, our results are in line with previous evidence indicating that distinct brain regions may have a higher intrinsic vulnerability to AD early pathophysiological alterations (Bero et al., 2011; Chiesa et al., 2019; Crossley et al., 2014; Hampel et al., 2019a).

#### *Potential utilization of PLS-VIP approach in resilience studies*

By contrast, We also found an apparent discrepancy between time points, with DMN and SaN being associated at baseline but not over time. A clinical explanation for these findings lies in the general and study-wise characteristic of our cohort.

Although SMC is a condition itself associated with increased risk for developing AD cognitive decline, the biology underlining the SMC clinical label, for instance, presence or not of brain A $\beta$  accumulation, is heterogeneous and longitudinal trajectories of SMC individuals may be different with some having or developing brain resilience, at the molecular and network level, and some other going toward multi-scale system failure and cognitive decline (Dubois et al., 2018; Hohman et al., 2016; Negash et al., 2013).

In the present study, only 4 individuals - out of 261 - included in the present study developed objective cognitive decline (MCI or dementia) within the 3-year follow-up (all of them have positive A $\beta$ -PET). As we have addressed in In line with previous INSIGHT-preAD data-driven publications, we argue that such rates of cognitive decline, lower than expected in a population at risk for AD [i.e., SMC plus signs of A $\beta$  accumulation] is partially explained by the average high education level and cognitive reserve of the INSIGHT-preAD participants, a cohort in which potential compensatory mechanisms have already been reported (Babiloni et al., 2020; Dubois et al., 2018; Gaubert et al., 2019). This cohort mostly embraces the Paris area and it is mainly represented by people who still engage in small post-retirement works, continuous social and intellectual activity (Babiloni et al., 2020; Cacciamani et al., 2020; Dubois et al., 2018).

In summary, we have not been surprised in encountering these our DMN-related divergent results and believe that this evidence-based conceptual construct can also explain the apparent DMN-related inconsistent association over time-points in our study. We have based our hypothesis on the presence of cognitive reserve-related resiliency dynamics in our cohort dataset by capitalizing on extensive evidence and data-driven conceptual frameworks

previously published ~~and proposed~~ (Babiloni et al., 2020; Dubois et al., 2018; Gaubert et al., 2019; Hohman et al., 2016; Negash et al., 2013).

In this conceptual framework lies the potential clinical value of our proposed study design. In fact, the PLS-based whole-brain approach could be used not only for investigating network dysfunction in AD trajectories but also resilience in individuals displaying incipient molecular signatures of AD or any other neurodegenerative disease.

Such speculation connects to our intention of carrying out a non-a-priori approach, like PLS-VIP, to facilitate the investigation of a broader set of brain functional networks and their association with AD pathophysiology, thus, enabling the identification of other network-network connection patterns involved in disease progression or compensation.

#### *No association between glucose metabolism and A $\beta$ accumulation according to the PLS analysis*

Our FDG-PET based results suggest that plasma A $\beta$ 42/A $\beta$ 40 ratio is not a suitable marker of neuronal metabolism that has been reported as a potential surrogate marker of neuronal loss (Dubois et al., 2014). To our knowledge, only one study assessed the association between A $\beta$ 42/A $\beta$ 40 ratio and FDG-PET in MCI/dementia pooled cohort (Pérez-Grijalba et al., 2019). By contrast, no results have been reported on cognitively healthy normal individuals at clinical and or biological risk for AD . Therefore, an interpretation of our data in light of the existing literature is hard to perform. However, it is conceivable to argue that the lack of FDG-PET signal with plasma A $\beta$ 42/A $\beta$ 40 ratio indicates that the latter is not a suitable marker for either neurodegeneration or disease progression.

#### *The PLS-VIP method main advantages for AD clinical research*

We believe that our workplan is easily replicable and shows good intrinsic operability. Of note, we used a set of variables with known covariance to test the performance of the modeling approach. The true potential of our approach is for exploratory purposes besides validation studies. PLS can be considered as a generalization of multiple regression since, for identical problem formulations, they both produce similar answers (Cramer, 1993). ~~But,~~ Unlike multiple regression, PLS can handle extensive datasets that may ~~are likely to~~ contain more predictors than subjects (Cramer, 1993; Krishnan et al., 2011). ~~A situation increasingly common in neurosciences due to significant progress in biomedical imaging and omics methods.~~

In addition, PLS is a very versatile method that provides relevant tools for different settings of clinical investigations. For instance, in AD clinical research, PLS was used for diagnostic classification tasks (Aguilar et al., 2014), omics studies (Lorenzi et al., 2018; Vardarajan et al., 2020; Xicota et al., 2019) and early longitudinal cognitive decline (Langbaum et al., 2020). The diversity of applications shows that PLS is a suitable tool for both hypothesis testing and explanatory model building. Likewise, PLS-VIP was used in AD studies to select variables predicting brain volume changes in AD (Thambisetty et al., 2011) or associated with AD biomarkers (Baldacci et al., 2020). PLS-VIP approach is not sensitive to multicollinearity among predictors, which is a remarkable advantage compared to conventional feature variable-selection method selection (Chong and Jun, 2005; Cramer, 1993; Palermo et al., 2009).

The Least Absolute Shrinkage and Selection Operator (LASSO) regression is another method previously used in AD clinical research for feature selection able to handle correlated variables. LASSO was used in gene based genome wide association studies to identify potential novel risk genes (Kohannim, 2012; Li et al., 2018; Yang et al., 2015) or relevant fluid biomarkers to Alzheimer's pathophysiology (Dayon et al., 2018). However, LASSO presents significant inconsistency among the variable selection (Zou and Hastie, 2005). Besides, while in PLS all features contribute to the construction of the components, LASSO and constraints all correlated variables but one to have null coefficients. So, among a set of correlated variables, LASSO regression i.e., the method selects only one feature and drops the others (Desboulets, 2018; Hastie et al., 2009). Elastic net regularization is a good alternative to LASSO that provides better performance and stability in variable selection (Zou and Hastie, 2005). However, with the elastic net, the coefficients' weight is distributed among the correlated variables, so when we interpret the model, the strength of the association is underrated. Overall, LASSO and Elastic net show good sparse property, which is appropriate for predictive models. In contrast, The most relevant advantage great benefit of PLS compared to other methods is not to keep all skip relevant associations, providing a complete nor lead to an incomplete overview of the process of interest, which is appropriate for explicative models and critical. A model providing a comprehensive framework of inter relation between multi-modal observations is critically crucial for interpreting the early pathophysiological dynamics process.

One main limitation of our approach is that we reduce statistic power when we split the dataset into training and test datasets. Thus, while we used a non a priori approach to explore all available hypotheses, we cannot exclude that subtle associations were missed. As

normally done in machine learning approaches, we split ~~But, by splitting~~ the dataset, ~~we~~ to increase the confidence in the significant findings. By contrast, such a step may reduce statistic power, thus hindering the detection of some subtle albeit clinically meaningful associations.

~~Statistical analysis typically compromises the number of hypotheses to explore and confidence in the results. When no assumptions are made about the data, then there is no reason to prefer one method over any other. The only way is to use strategies, like dataset splitting, to evaluate them (Wolpert, 1996).~~

### *Study limitations*

We acknowledge that different atlases, including cytoarchitectonic and probabilistic maps, have been published lately and some of them are expected to perform better, especially for those regions with no clear macro-anatomical landmarks. This methodological limitation explains why we did not include subcortical regions in the present study.

The present study does not include a long-term neuropsychological clinical follow-up of participants, which represents a limitation. Moreover, although education is widely considered a component of the cognitive reserve we thought not to overload our PLS-based approach and region models with too many covariates, considering that the dataset is not large enough.

To expand on the clinical potential of our approach, we set out to extend the multi-modal biomarker and neuropsychological follow-up of the individuals involved in the present study. In addition, we aim at expanding the dataset through a multi-centric study where we would use PLS to explore trajectories of decline versus resilience, also keeping education levels into model. This future study would include an independent validation cohort, the lack of which represents caveat itself. To compensate this issue, we carried out several additional analytical steps (training/test datasets, bootstrap, correction for multiple tests, and internal reproduction at different timepoints) to increase confidence in the findings. We also acknowledge the lack of a test cohort of MCI and dementia individuals with AD pathophysiology as a major caveat of our study since it may have supported data interpretation from a biological standpoint and to draw some clinical conclusions. In this sense, we set out to perform a large-scale longitudinal multi-center study including at least one discovery and one independent validation cohort spanning the entire AD continuum, and including SMC and MCI either converters or stable. We believe that this follow-up study is essential for the standardization and harmonization of our proposed analytical protocol, and at

the same time, to investigate whether our whole-brain approach may generate reliable predictive measures to employ in clinical trials and evolving healthcare practice.

## CONCLUSIONS

Our study shows that plasma A $\beta$ 42/A $\beta$ 40 ratio is negatively associated with several regional A $\beta$ -PET indexes at a cross-sectional and longitudinal level in SMC individuals. Leveraging the PLS-VIP computational power and using a non-a-priori strategy (i.e., hypothesis-free), we find several associations between plasma A $\beta$ 42/A $\beta$ 40 ratio and brain regions belonging to multiple large-scale functional networks, including networks normally not investigated in a-priori study designs for preclinical AD.

Of note, we do not suggest to set aside a priori hypothesis investigations but instead promote an integrated approach based on the notion that a-priori and non-a-priori investigations can be complementary and provide partially different information for clinical research. We propose that non-a-priori investigations should be employed in biomarker-guided exploratory studies conducted in preclinical populations to facilitate the understanding of early pathophysiological trajectories of neurodegenerative diseases and to identify vulnerable regions that may deserve specific attention for preventive strategies.

## CREDIT AUTHOR STATEMENT

**Pablo Lemercier:** Conceptualization, Methodology, Formal analysis, Data interpretation, Validation, Writing - original draft, Supervision, Writing - review & editing, **Andrea Vergallo:** Conceptualization, Methodology, Data interpretation, Validation, Writing - original draft, Supervision, Writing - review & editing, **Simone Lista:** Investigation, Data curation, Writing - review & editing, **Henrik Zetterberg:** Investigation, Data curation, Writing - review & editing, **Kaj Blennow:** Investigation, Data curation, Writing - review & editing, **Marie-Claude Potier:** Provided the APOE genotype assessment, Writing - review & editing, **Marie-Odile Habert:** Provided the PET biomarker assessment, Writing - review & editing, **François-Xavier Lejeune:** Conceptualization, Methodology, Formal analysis, Data interpretation, Writing - review & editing, **Bruno Dubois:** Investigation, Data curation, Project administration, **Stefan Teipell:** Investigation, Data curation, Project administration, Data interpretation, Writing - review & editing, and **Harald Hampel:** Investigation, Data curation, Project administration, Data interpretation, Writing - review & editing.

## ACKNOWLEDGMENTS

The research and this manuscript was part of the translational research program “**PHOENIX**”, awarded to **HH**, and administered by the Sorbonne University Foundation and sponsored by la *Fondation pour la Recherche sur Alzheimer*.

The study was promoted by INSERM in collaboration with ICM, IHU-A-ICM and Pfizer and has received support within the “*Investissement d’Avenir*” (ANR-10-AIHU-06) French program. The study was promoted in collaboration with the “CHU de Bordeaux” (coordination CIC EC7), the promoter of Memento cohort, funded by the Foundation Plan-Alzheimer. The study was further supported by AVID/Lilly.

CATI is a French neuroimaging platform funded by the French Plan Alzheimer (available at <http://cati-neuroimaging.com>).

**AV** is an employee of Eisai Inc. This work was performed during his previous position at Sorbonne University, Paris, France.

**HH** is an employee of Eisai Inc. This work has been performed during his previous position at Sorbonne University, Paris, France. At Sorbonne University he was supported by the AXA Research Fund, the “*Fondation partenariale Sorbonne Université*” and the “*Fondation pour la Recherche sur Alzheimer*”, Paris, France.

**KB** is supported by the Swedish Research Council (#2017-00915), the Alzheimer Drug Discovery Foundation (ADDF), USA (#RDAPB-201809-2016615), the Swedish Alzheimer Foundation (#AF-742881), Hjärfonden, Sweden (#FO2017-0243), the Swedish state under the agreement between the Swedish government and the County Councils, the ALF-agreement (#ALFGBG-715986), the European Union Joint Program for Neurodegenerative Disorders (JPND2019-466-236), and the National Institute of Health (NIH), USA, (grant #1R01AG068398-01).

**HZ** is a Wallenberg Scholar supported by grants from the Swedish Research Council (#2018-02532), the European Research Council (#681712), Swedish State Support for Clinical Research (#ALFGBG-720931), the Alzheimer Drug Discovery Foundation (ADDF), USA (#201809-2016862), the AD Strategic Fund and the Alzheimer's Association (#ADSF-21-831376-C, #ADSF-21-831381-C and #ADSF-21-831377-C), the Olav Thon Foundation, the Erling-Persson Family Foundation, Stiftelsen för Gamla Tjänarinnor, Hjärfonden, Sweden (#FO2019-0228), the European Union’s Horizon 2020 research and innovation programme under the Marie Skłodowska-Curie grant agreement No 860197 (MIRIADE), and the UK Dementia Research Institute at UCL.

#### **INSIGHT-preAD Study Group:**

Hovagim Bakardjian, Habib Benali, Hugo Bertin, Joel Bonheur, Laurie Boukadida, Nadia Boukerrou, Enrica Cavedo, Patrizia Chiesa, Olivier Colliot, Bruno Dubois, Marion Dubois, Stéphane Epelbaum, Geoffroy Gagliardi, Remy Genthon, Marie-Odile Habert, Harald Hampel, Marion Houot, Aurélie Kas, Foudil Lamari, Marcel Levy, Simone Lista, Christiane Metzinger, Fanny Mochel, Francis Nyasse, Catherine Poisson, Marie-Claude Potier, Marie Revillon, Antonio Santos, Katia Santos Andrade, Marine Sole, Mohmed Surtee, Michel Thiebaut de Schotten, Andrea Vergallo, Nadjia Younsi.

## Contributors to the Alzheimer Precision Medicine Initiative – Working Group (APMI-WG):

Mohammad AFSHAR (France), Lisi Flores AGUILAR (Canada), Leyla AKMAN-ANDERSON (USA), Joaquín ARENAS (Spain), Jesús ÁVILA (Spain), Claudio BABILONI (Italy), Filippo BALDACCI (Italy), Richard BATRLA (Switzerland), Norbert BENDA (Germany), Keith L. BLACK (USA), Kaj BLENNOW (Sweden), Arun L.W. BOKDE (Ireland), Ubaldo BONUCCELLI (Italy), Karl BROICH (Germany), Francesco CACCIOLA (Italy), Filippo CARACI (Italy), Giuseppe CARUSO (Italy), Juan CASTRILLO† (Spain), Enrica CAVEDO (France), Roberto CERAVOLO (Italy), Patrizia A. CHIESA (France), Massimo CORBO (Italy), Jean-Christophe CORVOL (France), Augusto Claudio CUELLO (Canada), Jeffrey L. CUMMINGS (USA), Herman DEPYPERE (Belgium), Bruno DUBOIS (France), Andrea DUGGENTO (Italy), Enzo EMANUELE (Italy), Valentina ESCOTT-PRICE (UK), Howard FEDEROFF (USA), Maria Teresa FERRETTI (Switzerland), Massimo FIANDACA (USA), Richard A. FRANK (USA), Francesco GARACI (Italy), Hugo GEERTS (USA), Ezio GIACOBINI (Switzerland), Filippo S. GIORGI (Italy), Edward J. GOETZL (USA), Manuela GRAZIANI (Italy), Marion HABERKAMP (Germany), Marie-Odile HABERT (France), Britta HÄNISCH (Germany), Harald HAMPEL (France), Karl HERHOLZ (UK), Felix HERNANDEZ (Spain), Bruno P. IMBIMBO (Italy), Dimitrios KAPOGIANNIS (USA), Eric KARRAN (USA), Steven J. KIDDLE (UK), Seung H. KIM (South Korea), Yosef KORONYO (USA), Maya KORONYO-HAMAOU (USA), Todd LANGEVIN (USA), Stéphane LEHÉRICY (France), Pablo LEMERCIER (France), Simone LISTA (France), Francisco LLAVERO (Spain), Jean LORENCEAU (France), Alejandro LUCÍA (Spain), Dalila MANGO (Italy), Mark MAPSTONE (USA), Christian NERI (France), Robert NISTICÒ (Italy), Sid E. O'BRYANT (USA), Giovanni PALERMO (Italy), George PERRY (USA), Craig RITCHIE (UK), Simone ROSSI (Italy), Amira SAIDI (Italy), Emiliano SANTARNECCHI (USA), Lon S. SCHNEIDER (USA), Olaf SPORNS (USA), Stefan TEIPEL (Germany), Nicola TOSCHI (Italy), Pedro L. VALENZUELA (Spain), Bruno VELLAS (France), Steven R. VERDOONER (USA), Andrea VERGALLO (France), Nicolas VILLAIN (France), Kelly VIRECOULON GIUDICI (France), Mark WATLING (UK), Lindsay A. WELIKOVITCH (Canada), Janet WOODCOCK (USA), Erfan YOUNESI (France), Henrik ZETTERBERG (Sweden), José L. ZUGAZA (Spain).

## CONFLICT OF INTEREST

**HH** is an employee of Eisai Inc. declares no competing financial interests related to the present article and his contribution to this article reflects entirely and only his own academic expertise on the matter. HH serves as Senior Associate Editor for the Journal Alzheimer's & Dementia and does not receive any fees or honoraria since May 2019; before May 2019 he had received lecture fees from Servier, Biogen and Roche, research grants from Pfizer, Avid, and MSD Avenir (paid to the institution), travel funding from Eisai, Functional Neuromodulation, Axovant, Eli Lilly and company, Takeda and Zinfandel, GE-Healthcare and Oryzon Genomics, consultancy fees from Qynapse, Jung Diagnostics, Cytox Ltd., Axovant, Anavex, Takeda and Zinfandel, GE Healthcare, Oryzon Genomics, and Functional Neuromodulation, and participated in scientific advisory boards of Functional Neuromodulation, Axovant, Eisai, Eli Lilly and company, Cytox Ltd., GE Healthcare, Takeda and Zinfandel, Oryzon Genomics and Roche Diagnostics.

He is inventor of the following patents as a scientific expert and has received no royalties:

- *In Vitro* Multiparameter Determination Method for The Diagnosis and Early Diagnosis of Neurodegenerative Disorders Patent Number: 8916388

- *In Vitro* Procedure for Diagnosis and Early Diagnosis of Neurodegenerative Diseases Patent Number: 8298784
- Neurodegenerative Markers for Psychiatric Conditions Publication Number: 20120196300
- *In Vitro* Multiparameter Determination Method for The Diagnosis and Early Diagnosis of Neurodegenerative Disorders Publication Number: 20100062463
- *In Vitro* Method for The Diagnosis and Early Diagnosis of Neurodegenerative Disorders Publication Number: 20100035286
- *In Vitro* Procedure for Diagnosis and Early Diagnosis of Neurodegenerative Diseases Publication Number: 20090263822
- *In Vitro* Method for The Diagnosis of Neurodegenerative Diseases Patent Number: 7547553
- CSF Diagnostic in Vitro Method for Diagnosis of Dementias and Neuroinflammatory Diseases Publication Number: 20080206797
- *In Vitro* Method for The Diagnosis of Neurodegenerative Diseases Publication Number: 20080199966
- Neurodegenerative Markers for Psychiatric Conditions Publication Number: 20080131921
- Method for diagnosis of dementias and neuroinflammatory diseases based on an increased level of procalcitonin in cerebrospinal fluid: Publication number: United States Patent 10921330

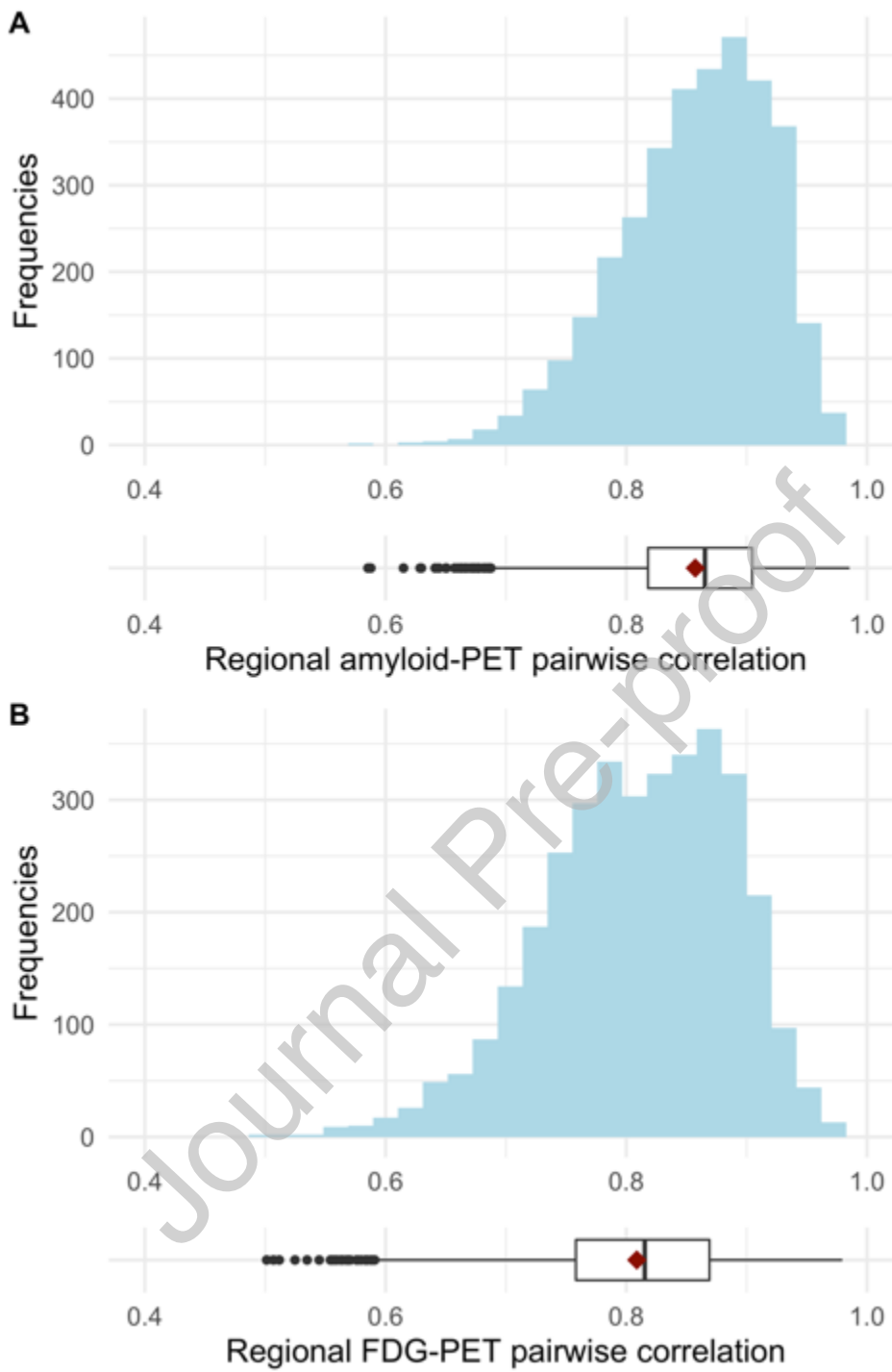
**AV** is an employee of Eisai Inc. AV declares no competing financial interests related to the present article and his contribution to this article reflects entirely and only his own academic expertise on the matter. AV does not receive any fees or honoraria since November 2019. Before November 2019 he had he received lecture honoraria from Roche, MagQu LLC, and Servier.

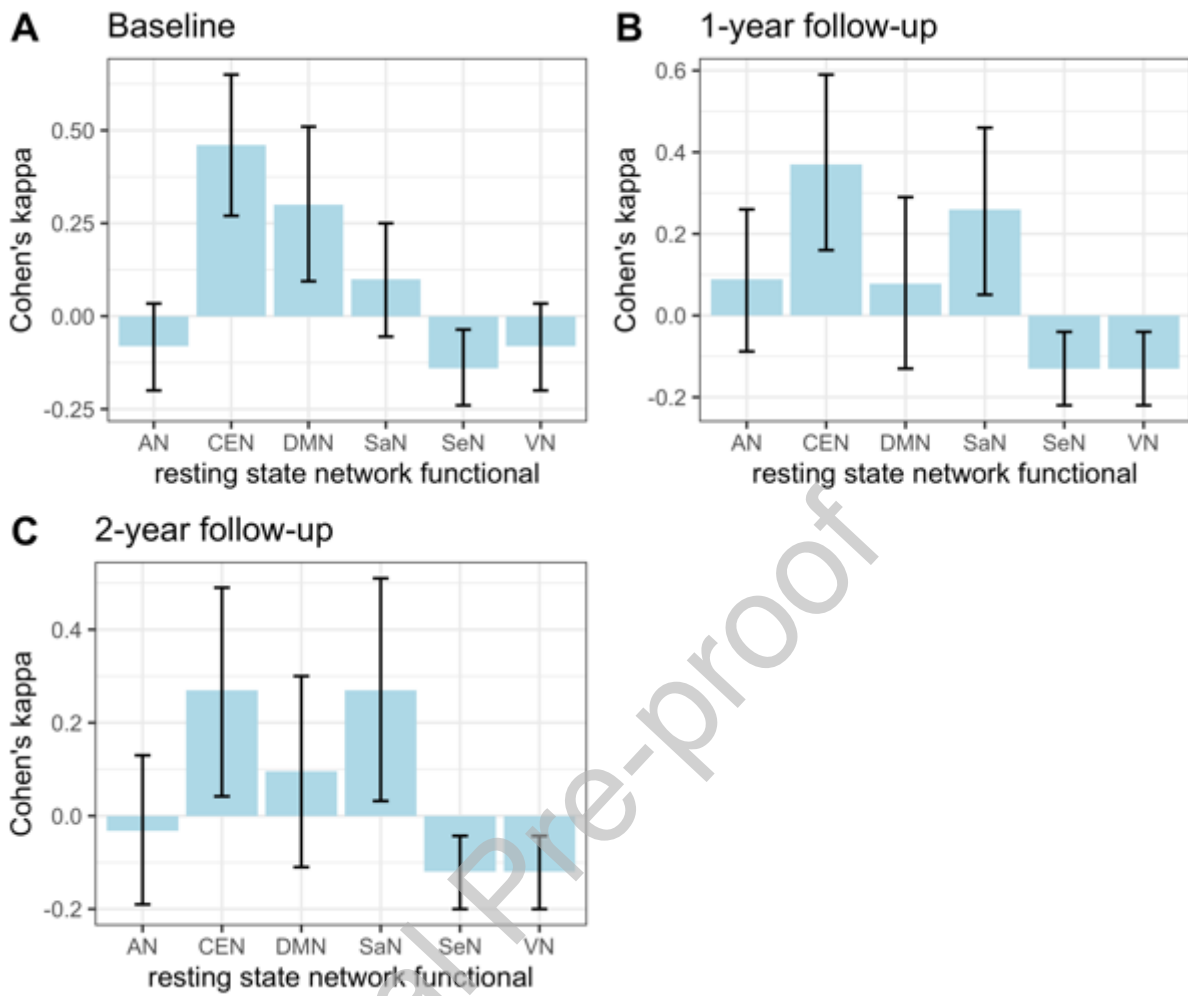
**SL** received lecture honoraria from Roche and Servier.

**PL, MCP, MOH, FXL, BD** declare no conflict of interest.

**KB** has served as a consultant, at advisory boards, or at data monitoring committees for Abcam, Axon, Biogen, JOMDD/Shimadzu, Julius Clinical, Lilly, MagQu, Novartis, Roche Diagnostics, and Siemens Healthineers, and is a co-founder of Brain Biomarker Solutions in Gothenburg AB (BBS), which is a part of the GU Ventures Incubator Program, outside the work presented in this paper.

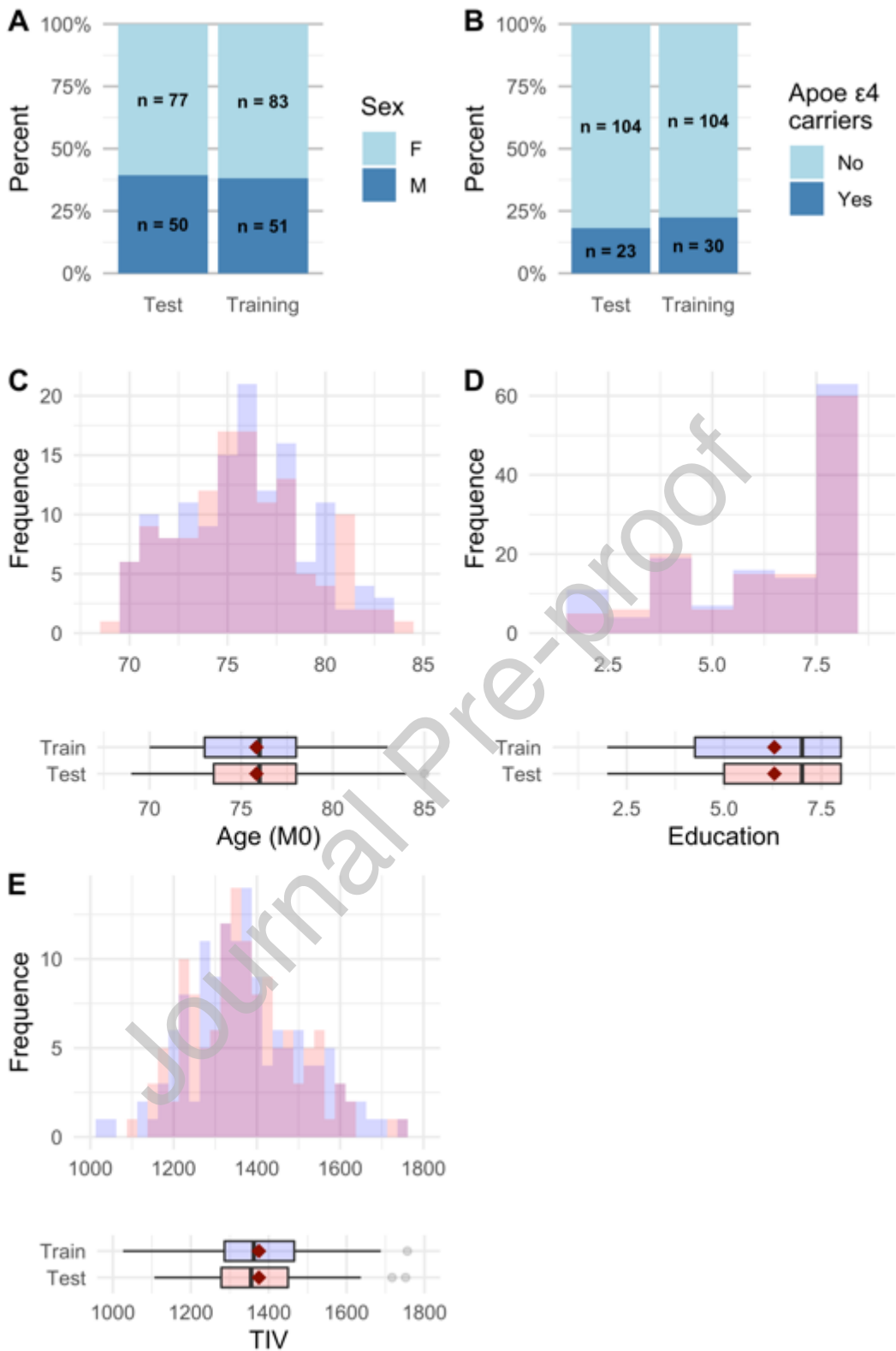
**HZ** has served at scientific advisory boards for Eisai, Denali, Roche Diagnostics, Wave, Samumed, Siemens Healthineers, Pinteon Therapeutics, Nervgen, AZTherapies and CogRx, has given lectures in symposia sponsored by Cellectricon, Fujirebio, Alzecure and Biogen, and is a co-founder of Brain Biomarker Solutions in Gothenburg AB (BBS), which is a part of the GU Ventures Incubator Program (outside submitted work).

**Figure 1.** Regional pairwise correlation

**Figure 2.** Cohen's Kappa between resting state network and amyloid-PET selected regions

Bar represent 95% confidence interval

Abbreviations: AN = auditory network, CEN = central executive network, DMN = default mode network, SaN = salience network, SeN = sensorimotor network, and VN = visual network

**Figure S1.** Description of training and test datasets

Abbreviations: APOE = apolipoprotein E, M0 = baseline visit, n = number of participants, and TIV = total intracranial volume

**Table 1.** Description of training and test databases at baseline

		<b>Training dataset N=134</b>	<b>Test dataset N=127</b>	<b>p-value</b>
<b>Age, mean <math>\pm</math> SD</b>		75.83 $\pm$ 3.23	75.81 $\pm$ 3.44	0.967
<b>Sex, n (%)</b>	Female	83 (61.9%)	77 (60.6%)	0.828
	Male	51 (38.1%)	50 (39.4%)	
<b>APOE <math>\epsilon</math>4 allele, n (%)</b>	Carriers	30 (22.4%)	23 (18.1%)	0.391
	Non-carriers	104 (77.6%)	104 (81.9%)	
<b>Education level, mean <math>\pm</math> SD</b>		6.29 $\pm$ 2.03	6.40 $\pm$ 1.90	0.651
<b>Total intracranial volume, mean <math>\pm</math> SD</b>		1375 $\pm$ 136	1369 $\pm$ 127	0.705

Student and Chi-squared tests are used to calculate p-values

Abbreviations: APOE = apolipoprotein E, N = number of participants, % = percent of participants, and SD = Standard deviation

**Table 2.** Association between A $\beta$ 42/A $\beta$ 40 ratio and amyloid-PET at baseline

Region	VIP score	Regression coefficient (SE)	p-value	Adjusted p-value	Cohen's f <sup>2</sup>
Angular left	1.04	-3.46 (1.25)	6.35e <sup>-3</sup>	6.99e <sup>-3</sup>	0.10
Angular right	1.21	-4.40 (1.24)	5.80e <sup>-4</sup>	1.46e <sup>-3</sup>	0.12
Calcarine left	1.04	-2.84 (0.98)	4.44e <sup>-3</sup>	5.59e <sup>-3</sup>	0.04
Cingulate Ant left	1.64	-4.32 (1.17)	3.47e <sup>-4</sup>	1.46e <sup>-3</sup>	0.11
Cingulate Ant right	1.29	-5.03 (1.20)	5.10e <sup>-5</sup>	9.20e <sup>-4</sup>	0.12
Cingulate Mid left	1.39	-3.89 (1.19)	1.41e <sup>-3</sup>	2.09e <sup>-3</sup>	0.10
Cingulate Mid right	1.41	-4.13 (1.14)	4.43e <sup>-4</sup>	1.46e <sup>-3</sup>	0.12
Cingulate Post left	1.27	-4.56 (1.29)	6.02e <sup>-4</sup>	1.46e <sup>-3</sup>	0.11
Cuneus left	1.10	-2.90 (1.01)	4.87e <sup>-3</sup>	5.92e <sup>-3</sup>	0.04
Frontal Inf Oper left	1.18	-3.29 (1.01)	1.52e <sup>-3</sup>	2.15e <sup>-3</sup>	0.10
Frontal Inf Orb 2 left	1.21	-3.85 (1.14)	9.83e <sup>-4</sup>	1.76e <sup>-3</sup>	0.06
Frontal Inf Orb 2 right	1.29	-3.71 (1.11)	1.05e <sup>-3</sup>	1.76e <sup>-3</sup>	0.13
Frontal Inf Tri left	1.16	-3.71 (1.11)	1.09e <sup>-3</sup>	1.76e <sup>-3</sup>	0.09
Frontal Med Orb left	1.57	-4.91 (1.33)	3.27e <sup>-4</sup>	1.46e <sup>-3</sup>	0.14
Frontal Med Orb right	1.26	-5.35 (1.28)	5.40e <sup>-5</sup>	9.20e <sup>-4</sup>	0.15
Frontal Mid 2 left	1.24	-4.28 (1.21)	5.62e <sup>-4</sup>	1.46e <sup>-3</sup>	0.11
Frontal Mid 2 right	1.35	-4.54 (1.21)	2.85e <sup>-4</sup>	1.46e <sup>-3</sup>	0.13
Frontal Sup 2 left	1.19	-4.30 (1.20)	5.05e <sup>-4</sup>	1.46e <sup>-3</sup>	0.10
Frontal Sup 2 right	1.20	-4.69 (1.18)	1.26e <sup>-4</sup>	1.27e <sup>-3</sup>	0.12
Frontal Sup Medial left	1.33	-4.20 (1.23)	8.68e <sup>-4</sup>	1.74e <sup>-3</sup>	0.12
Frontal Sup Medial right	1.21	-5.07 (1.29)	1.49e <sup>-4</sup>	1.27e <sup>-3</sup>	0.12
Insula right	1.06	-3.54 (0.97)	3.92e <sup>-4</sup>	1.46e <sup>-3</sup>	0.10
OFClat left	1.08	-4.26 (1.40)	2.96e <sup>-3</sup>	3.87e <sup>-3</sup>	0.07
OFCpost right	1.10	-3.04 (1.15)	8.99e <sup>-3</sup>	9.56e <sup>-3</sup>	0.12
Olfactory left	1.34	-2.46 (1.01)	1.63e <sup>-2</sup>	1.68e <sup>-2</sup>	0.11
Parietal Inf left	1.03	-3.34 (1.20)	6.37e <sup>-3</sup>	6.99e <sup>-3</sup>	0.12
Parietal Sup left	1.05	-3.34 (1.38)	1.71e <sup>-2</sup>	1.71e <sup>-2</sup>	0.09
Precuneus left	1.35	-4.00 (1.42)	5.80e <sup>-3</sup>	6.80e <sup>-3</sup>	0.08

Precuneus right	1.37	-4.25 (1.29)	$1.32e^{-3}$	$2.04e^{-3}$	0.10
Rectus left	1.43	-4.32 (1.26)	$8.00e^{-4}$	$1.71e^{-3}$	0.12
Rectus right	1.26	-4.49 (1.19)	$2.40e^{-4}$	$1.46e^{-3}$	0.13
SupraMarginal right	1.09	-3.78 (1.10)	$8.04e^{-4}$	$1.71e^{-3}$	0.10
Temporal Mid left	1.09	-3.13 (1.03)	$2.82e^{-3}$	$3.83e^{-3}$	0.10
Temporal Sup left	1.12	-2.98 (0.89)	$1.03e^{-3}$	$1.76e^{-3}$	0.09

VIP scores derive from the feature selection with PLS-VIP, while regression coefficient, p-value, adjusted p-value, and Cohen's  $f^2$  derived from the validation with linear models.

All models are adjusted for age, sex, and *APOE*  $\epsilon 4$  genotype. p-values refer to the test of regression coefficient. Adjusted p-values are calculated using false discovery rate correction.

Abbreviations: SE = Standard error and VIP = Variable Importance in Projection

**Table 3.** Association between A $\beta$ 42/A $\beta$ 40 ratio at M12 and amyloid-PET at M24

Region	VIP score	Regression coefficient (SE)	p-value	Adjusted p-value	Cohen's $f^2$
Cingulate Ant left	1.39	-5.12 (1.34)	2.46e <sup>-4</sup>	1.88e <sup>-3</sup>	0.17
Cingulate Ant right	1.38	-5.25 (1.33)	1.47e <sup>-4</sup>	1.88e <sup>-3</sup>	0.18
Frontal Inf Oper left	1.22	-3.21 (1.29)	1.43e <sup>-2</sup>	1.49e <sup>-2</sup>	0.10
Frontal Inf Oper right	1.13	-3.80 (1.25)	3.09e <sup>-3</sup>	4.19e <sup>-3</sup>	0.14
Frontal Inf Orb 2 left	1.02	-3.66 (1.32)	6.75e <sup>-3</sup>	7.67e <sup>-3</sup>	0.12
Frontal Inf Tri left	1.43	-3.69 (1.39)	9.21e <sup>-3</sup>	1.00e <sup>-2</sup>	0.10
Frontal Inf Tri right	1.40	-4.22 (1.37)	2.69e <sup>-3</sup>	3.95e <sup>-3</sup>	0.15
Frontal Med Orb left	1.32	-5.68 (1.51)	3.00e <sup>-4</sup>	1.88e <sup>-3</sup>	0.18
Frontal Med Orb right	1.05	-5.62 (1.49)	2.89e <sup>-4</sup>	1.88e <sup>-3</sup>	0.19
Frontal Mid 2 left	1.22	-4.20 (1.47)	5.07e <sup>-3</sup>	6.04e <sup>-3</sup>	0.12
Frontal Mid 2 right	1.29	-5.16 (1.49)	7.85e <sup>-4</sup>	2.45e <sup>-3</sup>	0.18
Frontal Sup 2 left	1.28	-4.47 (1.44)	2.45e <sup>-3</sup>	3.87e <sup>-3</sup>	0.13
Frontal Sup 2 right	1.23	-5.12 (1.43)	5.27e <sup>-4</sup>	2.20e <sup>-3</sup>	0.18
Frontal Sup Medial left	1.20	-4.71 (1.48)	1.93e <sup>-3</sup>	3.70e <sup>-3</sup>	0.13
Frontal Sup Medial right	1.25	-5.30 (1.50)	6.61e <sup>-4</sup>	2.36e <sup>-3</sup>	0.17
Insula left	1.06	-3.69 (1.17)	2.08e <sup>-3</sup>	3.71e <sup>-3</sup>	0.13
Insula right	1.11	-3.74 (1.20)	2.48e <sup>-3</sup>	3.87e <sup>-3</sup>	0.13
OFCmed left	1.34	-4.72 (1.44)	1.41e <sup>-3</sup>	3.20e <sup>-3</sup>	0.15
OFCpost left	1.03	-3.75 (1.28)	4.38e <sup>-3</sup>	5.48e <sup>-3</sup>	0.14
Rectus left	1.10	-5.30 (1.46)	4.40e <sup>-4</sup>	2.20e <sup>-3</sup>	0.18
Rectus right	1.26	-4.47 (1.38)	1.65e <sup>-3</sup>	3.44e <sup>-3</sup>	0.18
Temporal Mid left	1.10	-4.31 (1.29)	1.21e <sup>-3</sup>	3.03e <sup>-3</sup>	0.15
Temporal Pole Sup left	1.37	-2.95 (0.97)	3.19e <sup>-3</sup>	4.19e <sup>-3</sup>	0.18
Temporal Pole Sup right	1.08	-2.59 (1.07)	1.70e <sup>-2</sup>	1.70e <sup>-2</sup>	0.17
Temporal Sup left	1.07	-3.86 (1.15)	1.15e <sup>-3</sup>	3.03e <sup>-3</sup>	0.15

VIP scores derive from the feature selection with PLS-VIP, while regression coefficient, p-value, adjusted p-value, and Cohen's  $f^2$  derived from the validation with linear models.

All models are adjusted for age, sex, and *APOE*  $\epsilon 4$  genotype. p-values refer to the test of regression coefficient. Adjusted p-values are calculated using false discovery rate correction.

Abbreviations: SE = Standard error and VIP = Variable Importance in Projection

**Table 4.** Association between baseline A $\beta$ 42/A $\beta$ 40 ratio and amyloid-PET at M24

Region	VIP score	Regression coefficient (SE)	p-value	Adjusted p-value	Cohen's f <sup>2</sup>
Angular right	1.03	-2.82 (0.79)	0.001	0.004	0.08
Cingulate Ant left	1.20	-2.28 (0.72)	0.002	0.004	0.04
Cingulate Ant right	1.40	-2.24 (0.71)	0.002	0.004	0.05
Cingulate Mid right	1.01	-2.29 (0.68)	0.001	0.004	0.06
Frontal Inf Oper left	1.03	-1.96 (0.68)	0.005	0.005	0.04
Frontal Inf Oper right	1.16	-2.16 (0.65)	0.001	0.004	0.05
Frontal Inf Tri left	1.34	-2.02 (0.73)	0.007	0.007	0.04
Frontal Inf Tri right	1.34	-2.21 (0.72)	0.003	0.004	0.07
Frontal Mid 2 left	1.22	-2.19 (0.76)	0.005	0.005	0.04
Frontal Mid 2 right	1.43	-2.46 (0.76)	0.001	0.004	0.06
Frontal Sup 2 left	1.20	-2.26 (0.74)	0.003	0.004	0.04
Frontal Sup 2 right	1.34	-2.42 (0.72)	0.001	0.004	0.06
Frontal Sup Medial left	1.15	-2.55 (0.75)	0.001	0.004	0.03
Frontal Sup Medial right	1.10	-2.56 (0.76)	0.001	0.004	0.05
Insula right	1.08	-1.90 (0.62)	0.003	0.004	0.04
Occipital Inf left	1.03	-2.23 (0.79)	0.006	0.006	0.06
OFCpost left	1.05	-2.06 (0.68)	0.003	0.004	0.05
Rectus right	1.01	-2.22 (0.72)	0.003	0.004	0.07
Temporal Pole Sup left	1.39	-1.60 (0.52)	0.003	0.004	0.07

VIP scores derive from the feature selection with PLS-VIP, while regression coefficient, p-value, adjusted p-value, and Cohen's f<sup>2</sup> derived from the validation with linear models.

All models are adjusted for age, sex, and *APOE*  $\epsilon 4$  genotype. p-values refer to the test of regression coefficient. Adjusted p-values are calculated using false discovery rate correction.

Abbreviations: SE = Standard error and VIP = Variable Importance in Projection

**Table 5.** Association between A $\beta$ 42/A $\beta$ 40 ratio and FDG-PET at baseline

Region	VIP score	Regression coefficient (SE)	p-value	Adjusted p-value	Cohen's f <sup>2</sup>
Cingulate Post left	1.97	2.75 (2.62)	0.296	0.804	0.05
Cingulate Post right	2.27	1.52 (2.44)	0.533	0.804	0.07
Cuneus left	1.19	3.57 (2.54)	0.162	0.804	< 0.01
Frontal Med Orb left	1.42	1.10 (2.44)	0.653	0.804	0.01
Heschl right	1.59	-0.54 (2.70)	0.843	0.865	0.01
Hippocampus left	1.29	0.67 (1.03)	0.520	0.804	0.04
Hippocampus right	1.86	0.67 (0.99)	0.503	0.804	0.02
Lingual right	1.62	2.45 (2.17)	0.261	0.804	0.01
Occipital Inf right	1.78	2.89 (2.78)	0.301	0.804	0.01
Occipital Sup left	1.61	1.75 (2.83)	0.538	0.804	0.01
Olfactory right	1.70	0.39 (1.42)	0.783	0.865	0.02
Paracentral Lobule left	1.64	1.63 (2.30)	0.479	0.804	< 0.01
ParaHippocampal left	1.69	0.78 (1.01)	0.444	0.804	0.03
ParaHippocampal right	1.32	0.55 (1.08)	0.609	0.804	0.02
Temporal Pole Mid left	1.48	0.78 (1.43)	0.586	0.804	0.01
Temporal Pole Sup left	1.59	0.26 (1.55)	0.865	0.865	< 0.01

VIP scores derive from the feature selection with PLS-VIP, while regression coefficient, p-value, adjusted p-value, and Cohen's f<sup>2</sup> derived from the validation with linear models.

All models are adjusted for age, sex, and *APOE*  $\epsilon 4$  genotype. p-values refer to the test of regression coefficient. Adjusted p-values are calculated using false discovery rate correction.

Abbreviations: SE = Standard error and VIP = Variable Importance in Projection

**Table S1.** Correspondences between AAL labels and the literature-based functional MRI resting-state networks

<b>AAL labels</b>	<b>Functional MRI Resting-state networks</b>
Angular L	DMN, CEN
Angular R	DMN, CEN
Calcarine L	VN
Calcarine R	VN
Cingulate Ant L	DMN, SaN
Cingulate Ant R	DMN, SaN
Cingulate Mid L	DMN
Cingulate Mid R	DMN
Cingulate Post L	DMN
Cingulate Post R	DMN
Cuneus L	
Cuneus R	
Frontal Inf Oper L	CEN
Frontal Inf Oper R	
Frontal Inf Orb 2 L	DMN, CEN
Frontal Inf Orb 2 R	DMN
Frontal Inf Tri L	CEN
Frontal Inf Tri R	
Frontal Med Orb L	DMN, CEN
Frontal Med Orb R	DMN, CEN
Frontal Mid 2 L	DMN, CEN, SaN
Frontal Mid 2 R	DMN, CEN, SaN
Frontal Sup 2 L	CEN
Frontal Sup 2 R	DMN, CEN
Frontal Sup Medial L	CEN
Frontal Sup Medial R	DMN, CEN
Fusiform L	
Fusiform R	
Heschl L	AN
Heschl R	AN
Hippocampus L	DMN
Hippocampus R	DMN
Insula L	SaN
Insula R	SaN
Lingual L	
Lingual R	
Occipital Inf L	
Occipital Inf R	
Occipital Mid L	DMN, VN

Occipital Mid R	DMN, VN
Occipital Sup L	VN
Occipital Sup R	VN
OFCant L	DMN, CEN
OFCant R	DMN
OFClat L	DMN, CEN
OFClat R	DMN
OFCmed L	DMN, CEN
OFCmed R	DMN
OFCpost L	DMN, CEN
OFCpost R	DMN
Olfactory L	
Olfactory R	
Paracentral Lobule L	
Paracentral Lobule R	
ParaHippocampal L	DMN
ParaHippocampal R	DMN
Parietal Inf L	CEN
Parietal Inf R	CEN
Parietal Sup L	CEN
Parietal Sup R	
Postcentral L	SeN
Postcentral R	SeN
Precentral L	SeN
Precentral R	SeN
Precuneus L	DMN, CEN
Precuneus R	DMN
Rectus L	
Rectus R	
Rolandic Oper L	
Rolandic Oper R	
Supp Motor Area L	SaN, SeN
Supp Motor Area R	SaN, SeN
SupraMarginal L	
SupraMarginal R	CEN
Temporal Inf L	CEN
Temporal Inf R	
Temporal Mid L	CEN
Temporal Mid R	
Temporal Pole Mid L	CEN
Temporal Pole Mid R	
Temporal Pole Sup L	AN

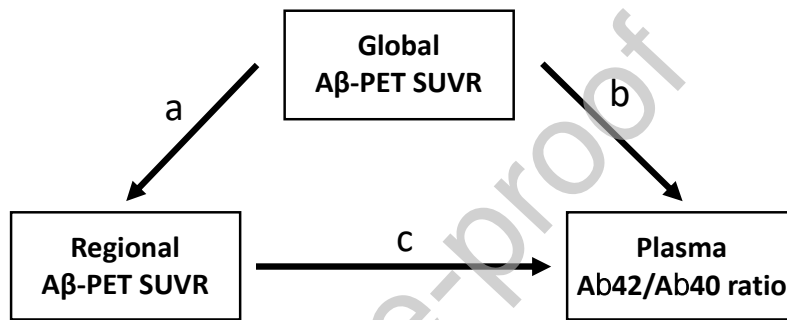
Temporal Pole Sup R	AN
Temporal Sup L	AN
Temporal Sup R	AN

The correspondence between the cortical regions of the AAL and the resting-state network atlases is based on our knowledge and through visual inspection (Shirer et al., 2012, doi: 10.1093/cercor/bhr099, Lee and Frangou, 2017; doi: 10.1038/s41598-017-16789-1). The definition of functional network components was made by grouping regions based on resting-state network atlas, available at [https://findlab.stanford.edu/functional\\_ROIs.html](https://findlab.stanford.edu/functional_ROIs.html))

Abbreviations: AAL = automated anatomical atlas, AN = auditory network, CEN = central executive network, DMN = default mode network, L = left, MRI = magnetic resonance imaging, OFC = orbitofrontal cortex, R = right, SaN = salience network, SeN = sensorimotor network and VN = visual network

Journal Pre-proof

Table S1-S2. Cross-sectional confounding analysis



Region	a			b			c		
	Regression coefficient (SE)	z-score	p-value	Regression coefficient (SE)	z-score	p-value	Regression coefficient (SE)	z-score	p-value
Angular left	1.24 (0.04)	31.94	< 0.01	-4.06e <sup>-3</sup> (0.04)	-0.11	0.91	-2.67e <sup>-2</sup> (0.03)	-0.93	0.35
Angular right	1.25 (0.03)	37.79	< 0.01	-1.56e <sup>-2</sup> (0.03)	-0.45	0.65	-1.71e <sup>-2</sup> (0.03)	-0.62	0.54
Calcarine left	1.02 (0.08)	13.02	< 0.01	-1.19e <sup>-2</sup> (0.03)	-0.45	0.65	-2.47e <sup>-2</sup> (0.03)	-0.82	0.41
Cingulate Ant left	1.05 (0.04)	26.04	< 0.01	1.50e <sup>-3</sup> (0.03)	0.06	0.95	-3.69e <sup>-2</sup> (0.02)	-1.65	0.10
Cingulate Ant right	1.06 (0.05)	23.34	< 0.01	-2.86e <sup>-2</sup> (0.04)	-0.78	0.43	-7.96e <sup>-3</sup> (0.03)	-0.26	0.79
Cingulate Mid left	1.08 (0.04)	26.37	< 0.01	1.52e <sup>-2</sup> (0.02)	0.63	0.53	-4.85e <sup>-2</sup> (0.02)	-2.17	0.03
Cingulate Mid right	1.08 (0.03)	38.80	< 0.01	9.19e <sup>-3</sup> (0.02)	0.37	0.71	-4.28e <sup>-2</sup> (0.02)	-2.00	0.05
Cingulate Post left	1.13 (0.04)	27.17	< 0.01	1.91e <sup>-2</sup> (0.03)	0.68	0.50	-4.95e <sup>-2</sup> (0.03)	-1.98	0.05
Cuneus left	1.02 (0.06)	17.43	< 0.01	-1.05e <sup>-2</sup> (0.03)	-0.40	0.69	-2.60e <sup>-2</sup> (0.03)	-0.95	0.34
Frontal Inf Oper left	1.04 (0.03)	39.88	< 0.01	-5.67e <sup>-2</sup> (0.05)	-1.16	0.25	1.90e <sup>-2</sup> (0.05)	0.39	0.70
Frontal Inf Orb 2 left	1.03 (0.04)	29.22	< 0.01	-3.98e <sup>-2</sup> (0.04)	-0.89	0.38	2.65e <sup>-3</sup> (0.04)	0.06	0.95
Frontal Inf Orb 2 right	1.04 (0.05)	22.19	< 0.01	7.38e <sup>-3</sup> (0.02)	0.37	0.71	-4.28e <sup>-2</sup> (0.02)	-2.17	0.03

Frontal Inf Tri left	1.11 (0.03)	43.08	< 0.01	-2.96e <sup>-2</sup> (0.05)	-0.60	0.55	-6.71e <sup>-3</sup> (0.05)	-0.15	0.88
Frontal Med Orb left	1.20 (0.05)	24.57	< 0.01	-4.66e <sup>-3</sup> (0.03)	-0.16	0.87	-2.70e <sup>-2</sup> (0.02)	-1.21	0.23
Frontal Med Orb right	1.23 (0.05)	25.24	< 0.01	-5.12e <sup>-2</sup> (0.04)	-1.18	0.24	1.15e <sup>-2</sup> (0.03)	0.36	0.72
Frontal Mid 2 left	1.16 (0.03)	36.01	< 0.01	-3.67e <sup>-2</sup> (0.05)	-0.70	0.49	-3.79e <sup>-4</sup> (0.05)	-0.01	0.99
Frontal Mid 2 right	1.18 (0.03)	36.38	< 0.01	1.64e <sup>-2</sup> (0.03)	0.47	0.64	-4.52e <sup>-2</sup> (0.03)	-1.43	0.15
Frontal Sup 2 left	1.12 (0.04)	27.23	< 0.01	-5.33e <sup>-3</sup> (0.03)	-0.17	0.87	-2.83e <sup>-2</sup> (0.03)	-0.94	0.35
Frontal Sup 2 right	1.12 (0.04)	30.05	< 0.01	3.58e <sup>-3</sup> (0.02)	0.16	0.88	-3.63e <sup>-2</sup> (0.02)	-1.74	0.08
Frontal Sup Medial left	1.12 (0.05)	21.10	< 0.01	2.40e <sup>-4</sup> (0.03)	0.01	0.99	-3.35e <sup>-2</sup> (0.03)	-1.22	0.22
Frontal Sup Medial right	1.14 (0.04)	25.83	< 0.01	1.88e <sup>-2</sup> (0.02)	0.76	0.45	-4.89e <sup>-2</sup> (0.02)	-2.07	0.04
Insula right	0.95 (0.03)	32.69	< 0.01	-9.76e <sup>-2</sup> (0.06)	-1.60	0.11	6.41e <sup>-2</sup> (0.06)	1.07	0.28
OFClat left	1.22 (0.04)	31.28	< 0.01	-5.37e <sup>-2</sup> (0.02)	-2.55	0.01	1.36e <sup>-2</sup> (0.01)	0.96	0.34
OFCpost right	0.95 (0.05)	19.89	< 0.01	-3.84e <sup>-2</sup> (0.02)	-2.00	0.05	1.37e <sup>-3</sup> (0.02)	0.09	0.93
Olfactory left	0.80 (0.04)	18.00	< 0.01	-4.72e <sup>-2</sup> (0.02)	-2.02	0.04	1.27e <sup>-2</sup> (0.03)	0.45	0.65
Parietal Inf left	1.08 (0.06)	18.68	< 0.01	-1.98e <sup>-2</sup> (0.02)	-0.92	0.36	-1.61e <sup>-2</sup> (0.02)	-0.94	0.35
Parietal Sup left	1.18 (0.08)	15.64	< 0.01	3.75e <sup>-3</sup> (0.02)	0.20	0.84	-3.45e <sup>-2</sup> (0.02)	-2.29	0.02
Precuneus left	1.27 (0.04)	28.50	< 0.01	3.65e <sup>-2</sup> (0.03)	1.17	0.24	-5.80e <sup>-2</sup> (0.03)	-2.21	0.03
Precuneus right	1.19 (0.04)	29.55	< 0.01	3.98e <sup>-2</sup> (0.04)	0.92	0.36	-6.47e <sup>-2</sup> (0.04)	-1.66	0.10
Rectus left	1.14 (0.05)	22.03	< 0.01	-3.26e <sup>-2</sup> (0.03)	-1.18	0.24	-3.93e <sup>-3</sup> (0.02)	-0.18	0.85
Rectus right	1.06 (0.06)	18.03	< 0.01	-7.26e <sup>-2</sup> (0.04)	-2.06	0.04	3.36e <sup>-2</sup> (0.03)	1.13	0.26
SupraMarginal right	1.06 (0.04)	29.85	< 0.01	-1.95e <sup>-2</sup> (0.02)	-0.82	0.42	-1.66e <sup>-2</sup> (0.02)	-0.73	0.46
Temporal Mid left	1.09 (0.02)	44.66	< 0.01	-3.78e <sup>-2</sup> (0.04)	-0.89	0.37	6.32e <sup>-4</sup> (0.04)	0.02	0.99
Temporal Sup left	0.94 (0.03)	29.29	< 0.01	-3.97e <sup>-3</sup> (0.03)	-0.15	0.88	-3.53e <sup>-2</sup> (0.03)	-1.29	0.20

All models are adjusted for age, sex, and *APOE*  $\epsilon 4$  genotype, p-values are estimated with bootstrap.

Abbreviations: SE = Standard error

**Table S2-S3.** Association between A $\beta$ 42/A $\beta$ 40 ratio at M12 and FDG-PET at M24

Region	VIP score	Regression coefficient (SE)	p-value	Adjusted p-value	Cohen's $f^2$
Angular left	1.23	-0.44 (2.88)	0.879	0.980	< 0.01
Angular right	1.15	-0.12 (3.19)	0.970	0.980	0.01
Calcarine left	1.33	-0.94 (2.82)	0.738	0.980	0.01
Calcarine right	1.86	0.07 (2.80)	0.980	0.980	0.01
Cingulate Ant right	1.03	0.14 (3.27)	0.966	0.980	0.01
Cingulate Mid left	1.01	-1.51 (2.58)	0.559	0.980	0.01
Cingulate Post left	1.31	-1.72 (2.72)	0.530	0.980	0.01
Cingulate Post right	1.23	-0.23 (3.23)	0.942	0.980	< 0.01
Frontal Inf Oper left	1.06	-1.05 (2.51)	0.678	0.980	0.01
Frontal Med Orb right	1.29	-0.98 (1.43)	0.495	0.980	0.09
Lingual right	1.29	-0.96 (2.48)	0.700	0.980	0.01
Occipital Sup right	1.10	-0.68 (3.15)	0.830	0.980	< 0.01
OFCant right	1.21	-2.90 (2.00)	0.150	0.895	0.07
OFCmed left	1.14	-1.09 (1.45)	0.455	0.980	0.07
OFCmed right	1.36	-1.91 (1.38)	0.170	0.895	0.05
OFCpost left	1.08	-1.35 (1.30)	0.302	0.980	0.05
OFCpost right	1.13	-2.19 (1.56)	0.165	0.895	0.09
Olfactory left	1.02	-0.97 (1.53)	0.527	0.980	0.01
Olfactory right	1.05	-0.83 (1.58)	0.600	0.980	0.01
Parietal Sup left	1.20	-0.91 (2.81)	0.747	0.980	< 0.01
Rectus left	1.15	-2.30 (1.29)	0.078	0.895	0.11

VIP scores derive from the feature selection with PLS-VIP, while regression coefficient, p-value, adjusted p-value, and Cohen's  $f^2$  derived from the validation with linear models.

All models are adjusted for age, sex, and *APOE*  $\epsilon 4$  genotype. p-values refer to the test of regression coefficient. Adjusted p-values are calculated using false discovery rate correction.

Abbreviations: SE = Standard error and VIP = Variable Importance in Projection

**Table S3-S4.** Association between baseline A $\beta$ 42/A $\beta$ 40 ratio and FDG-PET at M24

Region	VIP score	Regression coefficient (SE)	p-value	Adjusted p-value	Cohen's f <sup>2</sup>
Angular left	1.34	0.42 (1.33)	0.750	1.000	0.01
Angular right	1.32	0.31 (1.44)	0.833	1.000	0.01
Calcarine left	1.33	0.56 (1.28)	0.666	1.000	0.01
Calcarine right	1.82	0.51 (1.27)	0.690	1.000	0.01
Cingulate Post left	1.10	-0.49 (1.29)	0.706	1.000	0.02
Cingulate Post right	1.14	-0.39 (1.48)	0.792	1.000	0.01
Frontal Inf Oper left	1.07	0.07 (1.15)	0.955	1.000	0.01
Occipital Inf right	1.03	-0.28 (1.21)	0.819	1.000	0.01
Occipital Mid left	1.07	0.44 (1.31)	0.734	1.000	< 0.01
Occipital Sup left	1.08	5.80e-3 (1.57)	1.000	1.000	< 0.01
Occipital Sup right	1.12	-0.35 (1.42)	0.804	1.000	< 0.01
OFCant right	1.01	0.05 (1.03)	0.965	1.000	0.05
OFClat right	1.07	-1.10 (1.33)	0.410	1.000	0.14
OFCmed right	1.26	0.14 (0.76)	0.850	1.000	0.03
OFCpost right	1.04	-0.05 (0.78)	0.946	1.000	0.06
Postcentral right	1.03	-0.18 (1.15)	0.874	1.000	< 0.01

VIP scores derive from the feature selection with PLS-VIP, while regression coefficient, p-value, adjusted p-value, and Cohen's f<sup>2</sup> derived from the validation with linear models.

All models are adjusted for age, sex, and *APOE*  $\epsilon 4$  genotype. p-values refer to the test of regression coefficient. Adjusted p-values are calculated using false discovery rate correction.

Abbreviations: SE = Standard error and VIP = Variable Importance in Projection

## REFERENCES

- Abdi, H., Williams, L.J., 2013. Partial Least Squares Methods: Partial Least Squares Correlation and Partial Least Square Regression. pp. 549–579. [https://doi.org/10.1007/978-1-62703-059-5\\_23](https://doi.org/10.1007/978-1-62703-059-5_23)
- Agosta, F., Pievani, M., Geroldi, C., Copetti, M., Frisoni, G.B., Filippi, M., 2012. Resting state fMRI in Alzheimer's disease: beyond the default mode network. *Neurobiol. Aging* 33, 1564–1578. <https://doi.org/10.1016/j.neurobiolaging.2011.06.007>
- Aguilar, C., Muehlboeck, J.S., Mecocci, P., Vellas, B., Tsolaki, M., Kloszewska, I., Soinenen, H., Lovestone, S., Wahlund, L.O., Simmons, A., Westman, E., 2014. Application of a MRI based index to longitudinal atrophy change in Alzheimer disease, mild cognitive impairment and healthy older individuals in the AddNeuroMed cohort. *Front. Aging Neurosci.* 6, 1–12. <https://doi.org/10.3389/fnagi.2014.00145>
- Aisen, P.S., Cummings, J., Jack, C.R., Morris, J.C., Sperling, R., Frölich, L., Jones, R.W., Dowsett, S.A., Matthews, B.R., Raskin, J., Scheltens, P., Dubois, B., 2017. On the path to 2025: understanding the Alzheimer's disease continuum. *Alzheimers. Res. Ther.* 9, 60. <https://doi.org/10.1186/s13195-017-0283-5>
- Andrews-Hanna, J.R., Snyder, A.Z., Vincent, J.L., Lustig, C., Head, D., Raichle, M.E., Buckner, R.L., 2007. Disruption of Large-Scale Brain Systems in Advanced Aging. *Neuron* 56, 924–935. <https://doi.org/10.1016/j.neuron.2007.10.038>
- Arenaza-Urquijo, E.M., Vemuri, P., 2018. Resistance vs resilience to Alzheimer disease. *Neurology* 90, 695–703. <https://doi.org/10.1212/WNL.0000000000005303>
- Babiloni, C., Lopez, S., Del Percio, C., Noce, G., Pascarelli, M.T., Lizio, R., Teipel, S.J., González-Escamilla, G., Bakardjian, H., George, N., Cavedo, E., Lista, S., Chiesa, P.A., Vergallo, A., Lemercier, P., Spinelli, G., Grothe, M.J., Potier, M.-C., Stocchi, F., Ferri, R., Habert, M.-O., Fraga, F.J., Dubois, B., Hampel, H., 2020. Resting-State Posterior Alpha Rhythms Are Abnormal In Subjective Memory Complaint Seniors With Preclinical Alzheimer's Neuropathology And High Education Level: The Insight-Pread Study. *Neurobiol. Aging*. <https://doi.org/10.1016/j.neurobiolaging.2020.01.012>
- Badhwar, A.P., Tam, A., Dansereau, C., Orban, P., Hoffstaedter, F., Bellec, P., 2017. Resting-state network dysfunction in Alzheimer's disease: A systematic review and meta-analysis. *Alzheimer's Dement. Diagnosis, Assess. Dis. Monit.* 8, 73–85. <https://doi.org/10.1016/j.dadm.2017.03.007>
- Baldacci, F., Lista, S., Manca, M.L., Chiesa, P.A., Cavedo, E., Lemercier, P., Zetterberg, H., Blennow, K., Habert, M.-O., Potier, M.C., Dubois, B., Vergallo, A., Hampel, H., 2020.

Age and sex impact plasma NFL and t-Tau trajectories in individuals with subjective memory complaints: a 3-year follow-up study. *Alzheimers. Res. Ther.* 12, 147.

<https://doi.org/10.1186/s13195-020-00704-4>

Bateman, R.J., Xiong, C., Benzinger, T.L.S., Fagan, A.M., Goate, A., Fox, N.C., Marcus, D.S., Cairns, N.J., Xie, X., Blazey, T.M., Holtzman, D.M., Santacruz, A., Buckles, V., Oliver, A., Moulder, K., Aisen, P.S., Ghetti, B., Klunk, W.E., McDade, E., Martins, R.N., Masters, C.L., Mayeux, R., Ringman, J.M., Rossor, M.N., Schofield, P.R., Sperling, R.A., Salloway, S., Morris, J.C., 2012. Clinical and Biomarker Changes in Dominantly Inherited Alzheimer's Disease. *N. Engl. J. Med.* 367, 795–804.

<https://doi.org/10.1056/NEJMoA1202753>

Bero, A.W., Yan, P., Roh, J.H., Cirrito, J.R., Stewart, F.R., Raichle, M.E., Lee, J.-M., Holtzman, D.M., 2011. Neuronal activity regulates the regional vulnerability to amyloid- $\beta$  deposition. *Nat. Neurosci.* 14, 750–756. <https://doi.org/10.1038/nn.2801>

Brier, M.R., Thomas, J.B., Snyder, A.Z., Benzinger, T.L., Zhang, D., Raichle, M.E., Holtzman, D.M., Morris, J.C., Ances Dr., B.M., 2012. Loss of intranetwork and internetwork resting state functional connections with Alzheimer's disease progression. *J. Neurosci.* 32, 8890–8899. <https://doi.org/10.1523/JNEUROSCI.5698-11.2012>

Buckley, R.F., Maruff, P., Ames, D., Bourgeat, P., Martins, R.N., Masters, C.L., Rainey-Smith, S., Lautenschlager, N., Rowe, C.C., Savage, G., Villemagne, V.L., Ellis, K.A., 2016. Subjective memory decline predicts greater rates of clinical progression in preclinical Alzheimer's disease. *Alzheimer's Dement.* 12, 796–804.

<https://doi.org/10.1016/j.jalz.2015.12.013>

Buckley, R.F., Schultz, A.P., Hedden, T., Papp, K. V., Hanseeuw, B.J., Marshall, G., Sepulcre, J., Smith, E.E., Rentz, D.M., Johnson, K.A., Sperling, R.A., Chhatwal, J.P., 2017. Functional network integrity presages cognitive decline in preclinical Alzheimer disease. *Neurology* 89, 29–37. <https://doi.org/10.1212/WNL.0000000000004059>

Cacciamani, F., Sambati, L., Houot, M., Habert, M.-O., Dubois, B., Epelbaum, S., 2020. Awareness of cognitive decline trajectories in asymptomatic individuals at risk for AD. *Alzheimers. Res. Ther.* 12, 129. <https://doi.org/10.1186/s13195-020-00700-8>

Chand, G.B., Wu, J., Hajjar, I., Qiu, D., 2017. Interactions of the Saliency Network and Its Subsystems with the Default-Mode and the Central-Executive Networks in Normal Aging and Mild Cognitive Impairment. *Brain Connect.* 7, 401–412.

<https://doi.org/10.1089/brain.2017.0509>

Chen, J., Shu, H., Wang, Z., Zhan, Y., Liu, D., Liao, W., Xu, L., Liu, Y., Zhang, Z., 2016.

~~Convergent and divergent intranetwork and internetwork connectivity patterns in patients with remitted late life depression and amnesic mild cognitive impairment. Cortex 83, 194–211. <https://doi.org/10.1016/j.cortex.2016.08.001>~~

Chhatwal, J.P., Schultz, A.P., Johnson, K.A., Hedden, T., Jaimes, S., Benzinger, T.L.S., Jack, C., Ances, B.M., Ringman, J.M., Marcus, D.S., Ghetti, B., Farlow, M.R., Danek, A., Levin, J., Yakushev, I., Laske, C., Koeppe, R.A., Galasko, D.R., Xiong, C., Masters, C.L., Schofield, P.R., Kinnunen, K.M., Salloway, S., Martins, R.N., McDade, E., Cairns, N.J., Buckles, V.D., Morris, J.C., Bateman, R., Sperling, R.A., 2018. Preferential degradation of cognitive networks differentiates Alzheimer’s disease from ageing. *Brain* 141, 1486–1500. <https://doi.org/10.1093/brain/awy053>

Chiesa, P.A., Cavedo, E., Vergallo, A., Lista, S., Potier, M.-C., Habert, M.-O., Dubois, B., Thiebaut de Schotten, M., Hampel, H., INSIGHT-preAD study group, Alzheimer Precision Medicine Initiative (APMI), Bakardjian, H., Benali, H., Bertin, H., Bonheur, J., Boukadida, L., Boukerrou, N., Cavedo, E., Chiesa, P.A., Colliot, O., Dubois, B., Dubois, M., Epelbaum, S., Gagliardi, G., Genthon, R., Habert, M.-O., Hampel, H., Houot, M., Kas, A., Lamari, F., Levy, M., Lista, S., Metzinger, C., Mochel, F., Nyasse, F., Poisson, C., Potier, M.-C., Revillon, M., Santos, A., Andrade, K.S., Sole, M., Surtee, M., de Schotten, M.T., Vergallo, A., Younsi, N., Afshar, M., Aguilar, L.F., Akman-Anderson, L., Arenas, J., Avila, J., Babiloni, C., Baldacci, F., Batrla, R., Benda, N., Black, K.L., Bokde, A.L.W., Bonuccelli, U., Broich, K., Cacciola, F., Caraci, F., Castrillo, J., Cavedo, E., Ceravolo, R., Chiesa, P.A., Corvol, J.-C., Cuello, A.C., Cummings, J.L., Depypere, H., Dubois, B., Duggento, A., Emanuele, E., Escott-Price, V., Federoff, H., Ferretti, M.T., Fiandaca, M., Frank, R.A., Garaci, F., Geerts, H., Giorgi, F.S., Goetzl, E.J., Graziani, M., Haberkamp, M., Habert, M.-O., Hampel, H., Herholz, K., Hernandez, F., Kapogiannis, D., Karran, E., Kiddle, S.J., Kim, S.H., Koronyo, Y., Koronyo-Hamaoui, M., Langevin, T., Lehericy, S., Lucía, A., Lista, S., Lorenceau, J., Mango, D., Mapstone, M., Neri, C., Nisticó, R., O’Bryant, S.E., Palermo, G., Perry, G., Ritchie, C., Rossi, S., Saidi, A., Santarnecchi, E., Schneider, L.S., Sporns, O., Toschi, N., Verdooner, S.R., Vergallo, A., Villain, N., Welikovitch, L.A., Woodcock, J., Younesi, E., 2019. Differential default mode network trajectories in asymptomatic individuals at risk for Alzheimer’s disease. *Alzheimers. Dement.* 15, 940–950. <https://doi.org/10.1016/j.jalz.2019.03.006>

Chiesa, P.A., Houot, M., Vergallo, A., Cavedo, E., Lista, S., Potier, M.C., Zetterberg, H., Blennow, K., Vanmechelen, E., De Vos, A., Dubois, B., Hampel, H., 2020. Association

- of brain network dynamics with plasma biomarkers in subjective memory complainers. *Neurobiol. Aging* 88, 83–90. <https://doi.org/10.1016/j.neurobiolaging.2019.12.017>
- Chong, I.G., Jun, C.H., 2005. Performance of some variable selection methods when multicollinearity is present. *Chemom. Intell. Lab. Syst.* 78, 103–112. <https://doi.org/10.1016/j.chemolab.2004.12.011>
- Clancy, U., Gilmartin, D., Jochems, A.C.C., Knox, L., Doubal, F.N., Wardlaw, J.M., 2021. Neuropsychiatric symptoms associated with cerebral small vessel disease: a systematic review and meta-analysis. *The Lancet Psychiatry* 8, 225–236. [https://doi.org/10.1016/S2215-0366\(20\)30431-4](https://doi.org/10.1016/S2215-0366(20)30431-4)
- Cramer, R.D., 1993. Partial Least Squares (PLS): Its strengths and limitations. *Perspect. Drug Discov. Des.* 1, 269–278. <https://doi.org/10.1007/BF02174528>
- Crossley, N.A., Mechelli, A., Scott, J., Carletti, F., Fox, P.T., McGuire, P., Bullmore, E.T., 2014. The hubs of the human connectome are generally implicated in the anatomy of brain disorders. *Brain* 137, 2382–2395. <https://doi.org/10.1093/brain/awu132>
- Dayon, L., Núñez Galindo, A., Wojcik, J., Cominetti, O., Corthésy, J., Oikonomidi, A., Henry, H., Kussmann, M., Migliavacca, E., Severin, I., Bowman, G.L., Popp, J., 2018. Alzheimer disease pathology and the cerebrospinal fluid proteome. *Alzheimers. Res. Ther.* 10, 66. <https://doi.org/10.1186/s13195-018-0397-4>
- Desboulets, L., 2018. A Review on Variable Selection in Regression Analysis. *Econometrics* 6, 45. <https://doi.org/10.3390/econometrics6040045>
- Dubois, B., Epelbaum, S., Nyasse, F., Bakardjian, H., Gagliardi, G., Uspenskaya, O., Houot, M., Lista, S., Cacciamani, F., Potier, M.C., Bertrand, A., Lamari, F., Benali, H., Mangin, J.F., Colliot, O., Genthon, R., Habert, M.O., Hampel, H., Audrain, C., Auffret, A., Baldacci, F., Benakki, I., Bertin, H., Boukadida, L., Cavedo, E., Chiesa, P., Dauphinot, L., Dos Santos, A., Dubois, M., Durrleman, S., Fontaine, G., Genin, A., Glasman, P., Jungalee, N., Kas, A., Kilani, M., La Corte, V., Lehericy, S., Letondor, C., Levy, M., Lowrey, M., Ly, J., Makiese, O., Metzinger, C., Michon, A., Mochel, F., Poisson, C., Ratovohery, S., Revillon, M., Rojkova, K., Roy, P., Santos-Andrade, K., Schindler, R., Seux, L., Simon, V., Sole, M., Tandetnik, C., Teichmann, M., Thiebaut de Shotten, M., Younsi, N., 2018. Cognitive and neuroimaging features and brain  $\beta$ -amyloidosis in individuals at risk of Alzheimer's disease (INSIGHT-preAD): a longitudinal observational study. *Lancet Neurol.* 17, 335–346. [https://doi.org/10.1016/S1474-4422\(18\)30029-2](https://doi.org/10.1016/S1474-4422(18)30029-2)
- Dubois, B., Feldman, H.H., Jacova, C., Hampel, H., Molinuevo, J.L., Blennow, K., DeKosky,

- S.T., Gauthier, S., Selkoe, D., Bateman, R., Cappa, S., Crutch, S., Engelborghs, S., Frisoni, G.B., Fox, N.C., Galasko, D., Habert, M.-O., Jicha, G.A., Nordberg, A., Pasquier, F., Rabinovici, G., Robert, P., Rowe, C., Salloway, S., Sarazin, M., Epelbaum, S., de Souza, L.C., Vellas, B., Visser, P.J., Schneider, L., Stern, Y., Scheltens, P., Cummings, J.L., 2014. Advancing research diagnostic criteria for Alzheimer's disease: the IWG-2 criteria. *Lancet Neurol.* 13, 614–629. [https://doi.org/10.1016/S1474-4422\(14\)70090-0](https://doi.org/10.1016/S1474-4422(14)70090-0)
- Elman, J.A., Oh, H., Madison, C.M., Baker, S.L., Vogel, J.W., Marks, S.M., Crowley, S., O'Neil, J.P., Jagust, W.J., 2014. Neural compensation in older people with brain amyloid- $\beta$  deposition. *Nat. Neurosci.* 17, 1316–1318. <https://doi.org/10.1038/nn.3806>
- Fan, L.Y., Tzen, K.Y., Chen, Y.F., Chen, T.F., Lai, Y.M., Yen, R.F., Huang, Y.Y., Shiue, C.Y., Yang, S.Y., Chiu, M.J., 2018. The relation between brain amyloid deposition, cortical atrophy, and plasma biomarkers in amnesic mild cognitive impairment and Alzheimer's Disease. *Front. Aging Neurosci.* 10, 1–10. <https://doi.org/10.3389/fnagi.2018.00175>
- Fandos, N., Pérez-Grijalba, V., Pesini, P., Olmos, S., Bossa, M., Villemagne, V.L., Doecke, J., Fowler, C., Masters, C.L., Sarasa, M., 2017. Plasma amyloid  $\beta$  42/40 ratios as biomarkers for amyloid  $\beta$  cerebral deposition in cognitively normal individuals. *Alzheimer's Dement. Diagnosis, Assess. Dis. Monit.* 8, 179–187. <https://doi.org/10.1016/j.dadm.2017.07.004>
- Farrell, M.E., Chen, X., Rundle, M.M., Chan, M.Y., Wig, G.S., Park, D.C., 2018. Regional amyloid accumulation and cognitive decline in initially amyloid-negative adults. *Neurology* 91, e1809–e1821. <https://doi.org/10.1212/WNL.0000000000006469>
- Gaubert, S., Raimondo, F., Houot, M., Corsi, M.-C., Naccache, L., Diego Sitt, J., Hermann, B., Oudiette, D., Gagliardi, G., Habert, M.-O., Dubois, B., De Vico Fallani, F., Bakardjian, H., Epelbaum, S., 2019. EEG evidence of compensatory mechanisms in preclinical Alzheimer's disease. *Brain* 142, 2096–2112. <https://doi.org/10.1093/brain/awz150>
- Grothe, M.J., Teipel, S.J., 2016. Spatial patterns of atrophy, hypometabolism, and amyloid deposition in Alzheimer's disease correspond to dissociable functional brain networks. *Hum. Brain Mapp.* 37, 35–53. <https://doi.org/10.1002/hbm.23018>
- Habert, Marie Odile, Bertin, Hugo, Labit, M., Diallo, M., Marie, S., Martineau, K., Kas, Aurélie, Causse-Lemercier, Valérie, Bakardjian, Hovagim, Epelbaum, Stéphane, Chételat, G., Houot, M., Hampel, Harald, Dubois, Bruno, Mangin, J.F., Audrain, C.,

- Bakardjian, H., Benali, H., Bertin, H., Boukadida, L., Cacciamani, F., Causse-Lemercier, V., Cavedo, E., Chiesa, P., Colliot, O., Dos Santos, A., Dubois, B., Durrleman, S., Epelbaum, S., Gagliardi, G., Genthon, R., Habert, M. O., Hampel, H., Jungalee, N., Kas, A., Lehericy, S., Lamari, F., Letondor, C., Levy, M., Lista, S., Mochel, F., Nyasse, F., Poisson, C., Potier, M.C., Revillon, M., Rojkova, K., Roy, P., Santos-Andrade, K., Santos, A., Simon, V., Sole, M., Tandetnik, C., Thiebaud De Schotten, M., 2018. Evaluation of amyloid status in a cohort of elderly individuals with memory complaints: validation of the method of quantification and determination of positivity thresholds. *Ann. Nucl. Med.* 32, 75–86. <https://doi.org/10.1007/s12149-017-1221-0>
- Hempel, H., Lista, S., Neri, C., Vergallo, A., 2019a. Time for the systems-level integration of aging: Resilience enhancing strategies to prevent Alzheimer's disease. *Prog. Neurobiol.* 181, 101662. <https://doi.org/10.1016/j.pneurobio.2019.101662>
- Hempel, H., Vergallo, A., Perry, G., Lista, S., 2019b. The Alzheimer Precision Medicine Initiative. *J. Alzheimer's Dis.* 68, 1–24. <https://doi.org/10.3233/JAD-181121>
- Hampton, O.L., Buckley, R.F., Manning, L.K., Scott, M.R., Properzi, M.J., Peña-Gómez, C., Jacobs, H.I.L., Chhatwal, J.P., Johnson, K.A., Sperling, R.A., Schultz, A.P., 2020. Resting-state functional connectivity and amyloid burden influence longitudinal cortical thinning in the default mode network in preclinical Alzheimer's disease. *NeuroImage Clin.* 28, 102407. <https://doi.org/10.1016/j.nicl.2020.102407>
- Hastie, T., Tibshirani, R., Friedman, J., 2009. *The Elements of Statistical Learning*, Springer, Springer Series in Statistics. Springer New York, New York, NY. <https://doi.org/10.1007/978-0-387-84858-7>
- He, X., Qin, W., Liu, Y., Zhang, X., Duan, Y., Song, J., Li, K., Jiang, T., Yu, C., 2014. Abnormal salience network in normal aging and in amnesic mild cognitive impairment and Alzheimer's disease. *Hum. Brain Mapp.* 35, 3446–3464. <https://doi.org/10.1002/hbm.22414>
- Hohman, T.J., McLaren, D.G., Mormino, E.C., Gifford, K.A., Libon, D.J., Jefferson, A.L., Alzheimer's Disease Neuroimaging Initiative, 2016. Asymptomatic Alzheimer disease: Defining resilience. *Neurology* 87, 2443–2450. <https://doi.org/10.1212/WNL.0000000000003397>
- Jack, C.R., Bennett, D.A., Blennow, K., Carrillo, M.C., Dunn, B., Haeberlein, S.B., Holtzman, D.M., Jagust, W., Jessen, F., Karlawish, J., Liu, E., Molinuevo, J.L., Montine, T., Phelps, C., Rankin, K.P., Rowe, C.C., Scheltens, P., Siemers, E., Snyder, H.M., Sperling, R., Elliott, C., Masliah, E., Ryan, L., Silverberg, N., 2018. NIA-AA Research

- Framework: Toward a biological definition of Alzheimer's disease. *Alzheimer's Dement.* 14, 535–562. <https://doi.org/10.1016/j.jalz.2018.02.018>
- Johnson, W.E., Li, C., Rabinovic, A., 2007. Adjusting batch effects in microarray expression data using empirical Bayes methods. *Biostatistics* 8, 118–127. <https://doi.org/10.1093/biostatistics/kxj037>
- Kohannim, O., 2012. Discovery and replication of gene influences on brain structure using LASSO regression. *Front. Neurosci.* 6. <https://doi.org/10.3389/fnins.2012.00115>
- Krishnan, A., Williams, L.J., McIntosh, A.R., Abdi, H., 2011. Partial Least Squares (PLS) methods for neuroimaging: A tutorial and review. *Neuroimage* 56, 455–475. <https://doi.org/10.1016/j.neuroimage.2010.07.034>
- Landau, S.M., Harvey, D., Madison, C.M., Reiman, E.M., Foster, N.L., Aisen, P.S., Petersen, R.C., Shaw, L.M., Trojanowski, J.Q., Jack, C.R., Weiner, M.W., Jagust, W.J., 2010. Comparing predictors of conversion and decline in mild cognitive impairment. *Neurology* 75, 230–238. <https://doi.org/10.1212/WNL.0b013e3181e8e8b8>
- Langbaum, J.B., Ellison, N.N., Caputo, A., Thomas, R.G., Langlois, C., Riviere, M.-E., Graf, A., Lopez Lopez, C., Reiman, E.M., Tariot, P.N., Hendrix, S.B., 2020. The Alzheimer's Prevention Initiative Composite Cognitive Test: a practical measure for tracking cognitive decline in preclinical Alzheimer's disease. *Alzheimers. Res. Ther.* 12, 66. <https://doi.org/10.1186/s13195-020-00633-2>
- Li, X., Wang, H., Long, J., Pan, G., He, T., Anichtchik, O., Belshaw, R., Albani, D., Edison, P., Green, E.K., Scott, J., 2018. Systematic Analysis and Biomarker Study for Alzheimer's Disease. *Sci. Rep.* 8, 17394. <https://doi.org/10.1038/s41598-018-35789-3>
- Li, Y., Yao, Z., Yu, Y., Zou, Y., Fu, Y., Hu, B., 2019. Brain network alterations in individuals with and without mild cognitive impairment: parallel independent component analysis of AV1451 and AV45 positron emission tomography. *BMC Psychiatry* 19, 165. <https://doi.org/10.1186/s12888-019-2149-9>
- Lockhart, S.N., Schöll, M., Baker, S.L., Ayakta, N., Swinnerton, K.N., Bell, R.K., Mellinger, T.J., Shah, V.D., O'Neil, J.P., Janabi, M., Jagust, W.J., 2017. Amyloid and tau PET demonstrate region-specific associations in normal older people. *Neuroimage* 150, 191–199. <https://doi.org/10.1016/j.neuroimage.2017.02.051>
- Lorenzi, M., Altmann, A., Gutman, B., Wray, S., Arber, C., Hibar, D.P., Jahanshad, N., Schott, J.M., Alexander, D.C., Thompson, P.M., Ourselin, S., 2018. Susceptibility of brain atrophy to TRIB3 in Alzheimer's disease, evidence from functional prioritization in imaging genetics. *Proc. Natl. Acad. Sci.* 115, 3162–3167.

<https://doi.org/10.1073/pnas.1706100115>

McKhann, G.M., Knopman, D.S., Chertkow, H., Hyman, B.T., Jack, C.R., Kawas, C.H., Klunk, W.E., Koroshetz, W.J., Manly, J.J., Mayeux, R., Mohs, R.C., Morris, J.C., Rossor, M.N., Scheltens, P., Carrillo, M.C., Thies, B., Weintraub, S., Phelps, C.H., 2011. The diagnosis of dementia due to Alzheimer's disease: Recommendations from the National Institute on Aging-Alzheimer's Association workgroups on diagnostic guidelines for Alzheimer's disease. *Alzheimer's Dement.* 7, 263–269.

<https://doi.org/10.1016/j.jalz.2011.03.005>

Mehmood, T., Liland, K.H., Snipen, L., Sæbø, S., 2012. A review of variable selection methods in Partial Least Squares Regression. *Chemom. Intell. Lab. Syst.* 118, 62–69.

<https://doi.org/10.1016/j.chemolab.2012.07.010>

Mormino, E.C., Smiljic, A., Hayenga, A.O., H. Onami, S., Greicius, M.D., Rabinovici, G.D., Janabi, M., Baker, S.L., V. Yen, I., Madison, C.M., Miller, B.L., Jagust, W.J., 2011. Relationships between Beta-Amyloid and Functional Connectivity in Different Components of the Default Mode Network in Aging. *Cereb. Cortex* 21, 2399–2407.

<https://doi.org/10.1093/cercor/bhr025>

~~Myers, N., Pasquini, L., Göttler, J., Grimmer, T., Koch, K., Ortner, M., Neitzel, J., Mühlau, M., Förster, S., Kurz, A., Förstl, H., Zimmer, C., Wohlschläger, A.M., Riedl, V., Drzezga, A., Sorg, C., 2014. Within-patient correspondence of amyloid  $\beta$  and intrinsic network connectivity in Alzheimer's disease. *Brain* 137, 2052–2064.~~

~~<https://doi.org/10.1093/brain/awu103>~~

Nakamura, A., Kaneko, N., Villemagne, V.L., Kato, T., Doecke, J., Doré, V., Fowler, C., Li, Q.-X., Martins, R., Rowe, C., Tomita, T., Matsuzaki, K., Ishii, K.K., Ishii, K.K., Arahata, Y., Iwamoto, S., Ito, K., Tanaka, K., Masters, C.L., Yanagisawa, K., Rowe, C., Li, Q.-X., Fowler, C., Kato, T., Nakamura, A., Kaneko, N., Doecke, J., Yanagisawa, K., Arahata, Y., Ishii, K.K., Tanaka, K., Villemagne, V.L., Iwamoto, S., Ito, K., Matsuzaki, K., Doré, V., Tomita, T., Martins, R., Ishii, K.K., 2018. High performance plasma amyloid- $\beta$  biomarkers for Alzheimer's disease. *Nature* 554, 249–254.

<https://doi.org/10.1038/nature25456>

Negash, S., Xie, S., Davatzikos, C., Clark, C.M., Trojanowski, J.Q., Shaw, L.M., Wolk, D.A., Arnold, S.E., 2013. Cognitive and functional resilience despite molecular evidence of Alzheimer's disease pathology. *Alzheimers. Dement.* 9, e89-95.

<https://doi.org/10.1016/j.jalz.2012.01.009>

Palermo, G., Piraino, P., Zucht, H.-D., 2009. Performance of PLS regression coefficients in

- selecting variables for each response of a multivariate PLS for omics-type data. *Adv. Appl. Bioinform. Chem.* 2, 57–70. <https://doi.org/10.2147/aabc.s3619>
- Palmqvist, S., Janelidze, S., Stomrud, E., Zetterberg, H., Karl, J., Zink, K., Bittner, T., Mattsson, N., Eichenlaub, U., Blennow, K., Hansson, O., 2019. Performance of Fully Automated Plasma Assays as Screening Tests for Alzheimer Disease–Related  $\beta$ -Amyloid Status. *JAMA Neurol.* 76, 1060. <https://doi.org/10.1001/jamaneurol.2019.1632>
- Palmqvist, S., Schöll, M., Strandberg, O., Mattsson, N., Stomrud, E., Zetterberg, H., Blennow, K., Landau, S., Jagust, W., Hansson, O., 2017. Earliest accumulation of  $\beta$ -amyloid occurs within the default-mode network and concurrently affects brain connectivity. *Nat. Commun.* 8, 1214. <https://doi.org/10.1038/s41467-017-01150-x>
- Pérez-Grijalba, V., Romero, J., Pesini, P., Sarasa, L., Monleón, I., San-José, I., Arbizu, J., Martínez-Lage, P., Munuera, J., Ruiz, A., Tárraga, L., Boada, M., Sarasa, M., 2019. Plasma A $\beta$ 42/40 Ratio Detects Early Stages of Alzheimer’s Disease and Correlates with CSF and Neuroimaging Biomarkers in the AB255 Study. *J. Prev. Alzheimer’s Dis.* 6, 34–41. <https://doi.org/10.14283/jpad.2018.41>
- Perez-Nievas, B.G., Stein, T.D., Tai, H.-C., Dols-Icardo, O., Scotton, T.C., Barroeta-Espar, I., Fernandez-Carballo, L., de Munain, E.L., Perez, J., Marquie, M., Serrano-Pozo, A., Frosch, M.P., Lowe, V., Parisi, J.E., Petersen, R.C., Ikonovic, M.D., López, O.L., Klunk, W., Hyman, B.T., Gómez-Isla, T., 2013. Dissecting phenotypic traits linked to human resilience to Alzheimer’s pathology. *Brain* 136, 2510–2526. <https://doi.org/10.1093/brain/awt171>
- Rohart, F., Gautier, B., Singh, A., Lê Cao, K.-A., 2017. mixOmics: An R package for ‘omics feature selection and multiple data integration. *PLOS Comput. Biol.* 13, e1005752. <https://doi.org/10.1371/journal.pcbi.1005752>
- Rosseel, Y., 2012. lavaan : An R Package for Structural Equation Modeling. *J. Stat. Softw.* 48. <https://doi.org/10.18637/jss.v048.i02>
- Shirer, W.R., Ryali, S., Rykhlevskaia, E., Menon, V., Greicius, M.D., 2012. Decoding Subject-Driven Cognitive States with Whole-Brain Connectivity Patterns. *Cereb. Cortex* 22, 158–165. <https://doi.org/10.1093/cercor/bhr099>
- Teipel, S., Grothe, M.J., Zhou, J., Sepulcre, J., Dyrba, M., Sorg, C., Babiloni, C., 2016. Measuring cortical connectivity in Alzheimer’s disease as a brain neural network pathology: Toward clinical applications. *J. Int. Neuropsychol. Soc.* 22, 138–163. <https://doi.org/10.1017/S1355617715000995>
- Teipel, S.J., Dyrba, M., Chiesa, P.A., Sakr, F., Jelistratova, I., Lista, S., Vergallo, A.,

- Lemercier, P., Cavedo, E., Habert, M.O., Dubois, B., Hampel, H., Grothe, M.J., 2020. In vivo staging of regional amyloid deposition predicts functional conversion in the preclinical and prodromal phases of Alzheimer's disease. *Neurobiol. Aging* 93, 98–108. <https://doi.org/10.1016/j.neurobiolaging.2020.03.011>
- Thambisetty, M., Simmons, A., Hye, A., Campbell, J., Westman, E., Zhang, Y., Wahlund, L.O., Kinsey, A., Causevic, M., Killick, R., Kloszewska, I., Mecocci, P., Soininen, H., Tsolaki, M., Vellas, B., Spenger, C., Lovestone, S., 2011. Plasma biomarkers of brain atrophy in Alzheimer's disease. *PLoS One* 6, 1–7. <https://doi.org/10.1371/journal.pone.0028527>
- Timmers, T., Ossenkoppele, R., Verfaillie, S.C.J., van der Weijden, C.W.J., Slot, R.E.R., Wesselman, L.M.P., Windhorst, A.D., Wolters, E.E., Yaqub, M., Prins, N.D., Lammertsma, A.A., Scheltens, P., van der Flier, W.M., van Berckel, B.N.M., 2019. Amyloid PET and cognitive decline in cognitively normal individuals: the SCIENCE project. *Neurobiol. Aging* 79, 50–58. <https://doi.org/10.1016/j.neurobiolaging.2019.02.020>
- Van Etten, E.J., Bharadwaj, P.K., Nguyen, L.A., Hishaw, G.A., Trouard, T.P., Alexander, G.E., 2020. Right hippocampal volume mediation of subjective memory complaints differs by hypertension status in healthy aging. *Neurobiol. Aging* 94, 271–280. <https://doi.org/10.1016/j.neurobiolaging.2020.06.012>
- van Harten, A.C., Mielke, M.M., Swenson-Dravis, D.M., Hagen, C.E., Edwards, K.K., Roberts, R.O., Geda, Y.E., Knopman, D.S., Petersen, R.C., 2018. Subjective cognitive decline and risk of MCI: The Mayo Clinic Study of Aging. *Neurology* 91, e300–e312. <https://doi.org/10.1212/WNL.0000000000005863>
- van Harten, A.C., Visser, P.J., Pijnenburg, Y.A.L., Teunissen, C.E., Blankenstein, M.A., Scheltens, P., van der Flier, W.M., 2013. Cerebrospinal fluid A $\beta$ 42 is the best predictor of clinical progression in patients with subjective complaints. *Alzheimer's Dement.* 9, 481–487. <https://doi.org/10.1016/j.jalz.2012.08.004>
- Vardarajan, B., Kalia, V., Manly, J., Brickman, A., Reyes-Dumeyer, D., Lantigua, R., Ionita-Laza, I., Jones, D.P., Miller, G.W., Mayeux, R., 2020. Differences in plasma metabolites related to Alzheimer's disease, APOE  $\epsilon$ 4 status, and ethnicity. *Alzheimer's Dement. Transl. Res. Clin. Interv.* 6. <https://doi.org/10.1002/trc2.12025>
- Vergallo, A., Mégrét, L., Lista, S., Cavedo, E., Zetterberg, H., Blennow, K., Vanmechelen, E., De Vos, A., Habert, M.-O., Potier, M.-C., Dubois, B., Neri, C., Hampel, H., INSIGHT-preAD study group, Alzheimer Precision Medicine Initiative (APMI), 2019. Plasma

amyloid  $\beta$  40/42 ratio predicts cerebral amyloidosis in cognitively normal individuals at risk for Alzheimer's disease. *Alzheimers. Dement.* 15, 764–775.

<https://doi.org/10.1016/j.jalz.2019.03.009>

Veronese, M., Moro, L., Arcolin, M., Dipasquale, O., Rizzo, G., Expert, P., Khan, W., Fisher, P.M., Svarer, C., Bertoldo, A., Howes, O., Turkheimer, F.E., 2019. Covariance statistics and network analysis of brain PET imaging studies. *Sci. Rep.* 9, 1–15.

<https://doi.org/10.1038/s41598-019-39005-8>

Villemagne, V.L., Burnham, S., Bourgeat, P., Brown, B., Ellis, K.A., Salvado, O., Szoek, C., Macaulay, S.L., Martins, R., Maruff, P., Ames, D., Rowe, C.C., Masters, C.L., 2013. Amyloid  $\beta$  deposition, neurodegeneration, and cognitive decline in sporadic Alzheimer's disease: a prospective cohort study. *Lancet Neurol.* 12, 357–367.

[https://doi.org/10.1016/S1474-4422\(13\)70044-9](https://doi.org/10.1016/S1474-4422(13)70044-9)

Warrens, M.J., 2015. Five Ways to Look at Cohen's Kappa. *J. Psychol. Psychother.* 05.

<https://doi.org/10.4172/2161-0487.1000197>

Whittington, A., Sharp, D.J., Gunn, R.N., 2018. Spatiotemporal Distribution of  $\beta$ -Amyloid in Alzheimer Disease Is the Result of Heterogeneous Regional Carrying Capacities. *J. Nucl. Med.* 59, 822–827. <https://doi.org/10.2967/jnumed.117.194720>

Wickham, H., 2009. *ggplot2*. Springer New York, New York, NY.

<https://doi.org/10.1007/978-0-387-98141-3>

Wold, S., Johansson, E., Cocchi, M., 1993. PLS - Partial Least Squares Projections to Latent Structures, in: Kubinyi, H. (Ed.), *3D QSAR in Drug Design: Theory Methods and Applications*. Escom, pp. 523–550.

~~Wolpert, D.H., 1996. The Lack of A Priori Distinctions Between Learning Algorithms. *Neural Comput.* 8, 1341–1390. <https://doi.org/10.1162/neco.1996.8.7.1341>~~

Xicota, L., Ichou, F., Lejeune, F.-X., Colsch, B., Tenenhaus, A., Leroy, I., Fontaine, G., Lhomme, M., Bertin, H., Habert, M.-O., Epelbaum, S., Dubois, B., Mochel, F., Potier, M.-C., 2019. Multi-omics signature of brain amyloid deposition in asymptomatic individuals at-risk for Alzheimer's disease: The INSIGHT-preAD study. *EBioMedicine* 47, 518–528. <https://doi.org/10.1016/j.ebiom.2019.08.051>

Xu, Y., Goodacre, R., 2018. On Splitting Training and Validation Set: A Comparative Study of Cross-Validation, Bootstrap and Systematic Sampling for Estimating the Generalization Performance of Supervised Learning. *J. Anal. Test.* 2, 249–262.

<https://doi.org/10.1007/s41664-018-0068-2>

Yang, T., Wang, J., Sun, Q., Hibar, D.P., Jahanshad, N., Liu, L., Wang, Y., Zhan, L.,

Thompson, P.M., Ye, J., 2015. Detecting genetic risk factors for Alzheimer's disease in whole genome sequence data via Lasso screening, in: 2015 IEEE 12th International Symposium on Biomedical Imaging (ISBI). IEEE, pp. 985–989.

<https://doi.org/10.1109/ISBI.2015.7164036>

Zhao, Q., Sang, X., Metmer, H., Swati, Z. nawab N.K., Lu, J., 2019. Functional segregation of executive control network and frontoparietal network in Alzheimer's disease. *Cortex* 120, 36–48. <https://doi.org/10.1016/j.cortex.2019.04.026>

Zhou, J., Greicius, M.D., Gennatas, E.D., Growdon, M.E., Jang, J.Y., Rabinovici, G.D., Kramer, J.H., Weiner, M., Miller, B.L., Seeley, W.W., 2010. Divergent network connectivity changes in behavioural variant frontotemporal dementia and Alzheimer's disease. *Brain* 133, 1352–1367. <https://doi.org/10.1093/brain/awq075>

Zou, H., Hastie, T., 2005. Regularization and variable selection via the elastic net. *J. R. Stat. Soc. Ser. B Stat. Methodol.* 67, 301–320. <https://doi.org/10.1111/j.1467-9868.2005.00503.x>